Reprinted from ANNALS OF PHYSICS
Vol. 122, No. 1, September 15, 1979
Printed in Belgium

Quantum Maps

M. V. BERRY*

H. H. Wills Physics Laboratory, Tyndall Avenue, Bristol BS8 1TL, United Kingdom

N. L. BALAZS*

Department of Physics, State University of New York at Stony Brook, New York 11794

M. TABOR†

Noyes Chemical Laboratory, School of Chemical Sciences, Urbana, Illinois 61801

AND

A. VOROS

Service de Physique Théorique, Centre d'Études Nucléaires de Saclay, B.P. No. 2, 91190 Gif-sur-Yvette, France

Received November 3, 1978

We quantize area-preserving maps M of the phase plane q, p by devising a unitary operator $\hat{U}$ transforming states $|\psi_n\rangle$ into $|\psi_{n+1}\rangle$. The result is a system with one degree of freedom q on which to study the quantum implications of generic classical motion, including stochasticity. We derive exact expressions for the equation iterating wavefunctions $\psi_n(q)$, the propagator for Wigner functions $W_n(q, p)$, the eigenstates of the discrete analog of the quantum harmonic oscillator, and general complex Gaussian wave packets iterated by a $\hat{U}$ derived from a linear M. For $|\psi_n\rangle$ associated with curves $\mathscr{C}_n$ in q, p, we derive a semiclassical theory for evolving states and stationary states, analogous to the familiar WKB method. This theory breaks down when $\mathscr{C}_n$ gets so complicated as to develop convolutions of area $\hbar$ or smaller. Such complication is generic; its principal morphologies are "whorls" and "tendrils," associated respectively with elliptic and hyperbolic fixed points of M. Under $\hat{U}$, $\psi_n(q)$ eventually transforms into a new sort of wave that no longer perceives the details of $\mathscr{C}_n$. For all regimes, however, the smoothed $|\psi_n(q)|^2$ appears semiclassically appears to be given accurately by the smoothed projection of $\mathscr{C}_n$ onto the q axis, both smoothings being over a de Broglie wavelength. The classical, quantum, and semiclassical theory is illustrated by computations on the discrete quartic oscillator map. We display for the first time stochastic wavefunctions, dominated by dense clusters of caustics and characterized by multiple scales of oscillation.

* Research supported in part by the NSF.

† Present address: Noyes Laboratory of Chemical Physics, Department of Chemistry, California Institute of Technology, Pasadena, Calif. 91125.

0003-4916/79/100026-38$05.00/0

1. Introduction

Interest in semiclassical quantum mechanics has revived as a result of recent developments in classical mechanics. These concern generic bound systems governed by a time-independent Hamiltonian and whose number N of degrees of freedom exceeds unity. It is known [1–4] that motion in the $2N$-dimensional phase space is infinitely complictated, in the following sense: Some orbits wind smoothly round N-dimensional tori, while other orbits wander stochastically in manifolds of higher dimensionality such as $2N - 1$-dimensional hypersurfaces of constant energy; the two types of orbit can be intricately interwoven like the rationals among the reals. Extreme cases are integrable systems, where all orbits are confined to tori by the existence of N smooth constants of motion, and ergodic systems, where almost all orbits explore their energy surfaces.

It was realized long ago by Einstein [5] that to these different sorts of classical motion there must correspond different sorts of quantum state, whose difference becomes more pronounced in the semiclassical limit, that is, as $\hbar$ gets smaller. Today, the semiclassical mechanics of integrable regions in phase space is well understood [6–9]; the tori form a basis for quantization [15a, 16, 17], generalizing the Bohr–Sommerfeld rules for separable systems and the WKB method for one-dimensional systems. But for the quantum states in stochastic regions of phase space there is no such firm understanding, only some speculations [10–13, 40, 41] and some exploratory computations [14, 15b, 19].

For studying the quantum mechanics corresponding to generic classical motion it is obviously desirable to use the simplest possible model. Previously this was thought to be motion of a point mass in a two-dimensional potential (with insufficient symmetry to give a global constant of motion additional to the energy). One-dimensional systems seemed too simple since constancy of the energy is enough to constrain the motion to one-dimensional tori (contours of the Hamiltonian) in the two-dimensional phase plane. On the other hand, discrete area-preserving mappings of the phase plane onto itself can exhibit richly complicated behavior [3, 4, 18]: invariant curves (tori) on all scales, separated by stochastic "seas" formed by area-filling chaotic orbits. Such generic discrete maps are commonly employed as a device for studying systems with two degrees of freedom; they are generated when orbits repeatedly intersect a two-dimensional section of the three-dimensional constant-energy hypersurface.

In this paper we present direct quantization of a large class of generic area-preserving mappings of the plane q, p, thus producing a model where a wavefunction $\psi(q)$ depending on just one coordinate q can exhibit generic semiclassical behavior including quantum stochasticity. Corresponding to the classical map is the quantum map, generated by a unitary operator $\hat{U}$ transforming states $|\psi\rangle$. This is a discrete transformation: it is not strictly necessary to imagine a smooth evolution between states. However, it is helpful to do so, and indeed both classical and quantum maps are derived from a Hamiltonian that is periodic in time with period T, taking shapshots of the system at times nT where n is integral [19]. The maps are so constructed

that the classical system is integrable when $T = 0$; thus T is a perturbation parameter corresponding to turning on stochasticity.

We obtain some exact analytical results, including an integral equation for transforming wavefunctions $\psi(q)$, propagators for transforming Wigner functions $W(q, p)$ in the quantum phase plane q, p, quantum eigenfunctions and eigenvalues for stable linear maps (discrete harmonic oscillators), and a description of the evolution of Gaussian wave packets in unstable linear maps (discrete parabolic potential barriers and wells).

Semiclassical approximations are obtained for waves transforming under the quantum map, and also for the eigenvalues of quantum states associated with integrable regions of the map. The iteration of curves (rather than points) under the classical map turns out to be important; after many iterations curves typically develop complicated convolutions, whose morphology we show to be dominated by "whorls" and tendrils," associated respectively with stable and unstable fixed points of the classical map.

A computational study is made of the mapping of wavefunctions, starting with an initial state $\psi_0(q)$. As expected, the iterates of ψ_0 are very different according to whether the initial classical curve representing ψ_0 lies in an integrable or a stochastic region of the map. In particular, stochastic wavefunctions are here presented for the first time. They are characterized by the simultaneous presence of many scales of oscillation and dominated by clusters of caustics. A semiclassical theory for the probability density $|\psi_n(q)|^2$, based on the iteration of the classical curve representing $\psi_0(q)$, gives good numerical agreement with the exactly computed $|\psi_n(q)|^2$, even in highly stochastic regions.

2. Discrete Anharmonic Oscillator Quantum Maps

Let a quantum state $|\psi_n\rangle$ be produced by n applications of a unitary operator $\hat{U}$ to an initial state $|\psi_0\rangle$, so that

$$|\psi_{n+1}\rangle = \hat{U}\,|\psi_n\rangle. \tag{2.1}$$

We consider $\hat{U}$ to depend on the (one-dimensional) position and momentum operators $\hat{q}$ and $\hat{p}$ but not on n. In the position representation, wavefunctions $\psi(q)$ evolve according to

$$\psi_{n+1}(q') = \int_{-\infty}^{\infty} dq' \langle q \,|\, \hat{U} \,|\, q' \rangle\, \psi_n(q'). \tag{2.2}$$

The eigenvalues of $\hat{U}$ must lie on the unit circle, so $|\phi\rangle$ is an eigenstate if

$$\hat{U}\,|\phi\rangle = e^{-i\alpha/\hbar}\,|\phi\rangle, \tag{2.3}$$

where α is real (and is proportional to what has been called the "quasi-energy" [36]).

The quantum map (2.1) is defined by the operator $\hat{U}$. We wish to choose a $\hat{U}$ whose classical analog is a given area-preserving map M in the phase plane $X \equiv (q, p)$, defined by

$$X_{n+1} = M(X_n). \tag{2.4}$$

The map M is the analog of Hamilton's equations for a continuously evolving system, and (2.1) is the analog of Schrödinger's equation. There is no unique prescription for quantization, starting from classical mechanics, so we devise a class of sytems for which $\hat{U}$ and M can be constructed using conventional rules and are both simple.

For these maps the quantum mechancis is governed by a time-dependent Hamiltonian operator $\hat{H} = H(\hat{q}, \hat{p}, t)$, periodic with period T, whose time-average $\bar{H}(\hat{q}, \hat{p})$ describes a particle of mass μ moving in a potential $V(\hat{q})$, namely,

$$\bar{H}(\hat{q}, \hat{p}) = \hat{p}^2/2\mu + V(\hat{q}). \tag{2.5}$$

The particular time dependence of $\hat{H}$ is

$$\begin{aligned} \hat{H}(\hat{q}, \hat{p}, t) &= \hat{p}^2/2\mu\gamma \qquad (0 < t < \gamma T) \\ &= V(\hat{q})/(1 - \gamma) \qquad (\gamma T < t < T), \end{aligned} \tag{2.6}$$

corresponding to a sequence of purely "kinetic" and purely "potential" motions in which alternately the force is switched off and the mass made infinite. When γ is close to unity the motion is free apart from periodic impulses; it has been studied before for the case where $\hat{q}$ is an angle operator [19] and termed the "kicked quantum rotator," and for the case where $V(\hat{q})$ is harmonic [20] which describes paraxial wave propagation through a series of ideal thin lenses.

The operator $\hat{U}$ for the quantum map will describe the effect of $\hat{H}$ from $t = 0$ to $t = T$. Schrödinger's equation is easily solved, and gives

$$\hat{U} = e^{-iV(\hat{q})T/\hbar} e^{-i\hat{p}^2T/2\mu\hbar}, \tag{2.7}$$

which does not depend on γ. In q representation the matrix elements of $\hat{U}$ are

$$\langle q \mid \hat{U} \mid q' \rangle = \left(\frac{\mu}{2\pi\hbar T}\right)^{1/2} e^{i[-\pi/4 - V(q)T/\hbar + \mu(q-q')^2/2\hbar T]}, \tag{2.8}$$

showing that $\hat{U}$ is not a symmetric operator and so has complex eigenfunctions. $\hat{U}$ could easily be symmetrized, but at the cost of complicating the corresponding classical map; therefore we work with the unsymmetrical form. From (2.2), quantum wavefunctions transform according to the integral equation

$$\psi_{n+1}(q) = \left(\frac{\mu}{2\hbar T\pi}\right)^{1/2} e^{-i\pi/4 - iV(q)T/\hbar} \int_{-\infty}^{\infty} dq'\, e^{i\mu(q-q')^2/2\hbar T} \psi_n(q'). \tag{2.9}$$

The classical motion is governed by the Hamiltonian (2.6), with the operators $\hat{q}$ and $\hat{p}$ replaced by conjugate variables q, p. Between $t = nT$ and $t = (n+1)T$ the motion as governed by Hamilton's equations is a map of the phase plane onto itself which we take as M. Elementary calculation gives this classical map as

$$M: \begin{aligned} q_{n+1} &= q_n + p_n T/\mu \\ p_{n+1} &= p_n - TV'(q_{n+1}), \end{aligned} \tag{2.10}$$

where the prime denotes differentiation. As with the quantum map (2.7), this does not involve γ. M has determinant unity and so is area preserving as all Hamiltonian transformations must be. This map is the composition of two simple shears of the phase plane, first in the q direction and then in the p direction.

In the limit $T \to 0$ both quantum and classical maps become infinitesimal transformations. Then it is not hard to show that (2.9) reduces to the ordinary time-dependent Schrödinger equation and (2.10) reduces to Hamilton's equations, for the continuous evolution of the system in the average Hamiltonian $\bar{H}$ [Eq. (2.5)]. The classical motion is integrable in this case. For finite T, however, M is a generic map if $V(q)$ is generic, with the usual hierarchies of fixed points surrounded by invariant curves or stochastic "seas" (see Fig. 9a). (If $V(q)$ is a polynomial, the nonintegrability of M can be established by elementary methods like those used for Cremona transformations [21].) Therefore, T is a perturbation parameter whose increase destroys more and more of the invariant curves that M possesses when $T = 0$ (and which are simply contours of $\bar{H}$).

We want mainly to treat bound systems, so we take $V(q)$ as a potential well, with a minimum at $q = 0$, thus making the imperturbed system an anharmonic oscillator, which is certainly bound. When $T > 0$, these maps possess a bound region near the origin of the phase plane, but, in all the nontrivial cases we have studied, initial points $q_0 p_0$ sufficiently far from the origin eventually excape, that is, they iterate to infinity under M. Obvious standard maps are

$$V(q) = Aq^{2k}/2k \qquad (k = 1, 2, 3, \ldots), \tag{2.11}$$

for which the scaling

$$q \equiv x\left(\frac{\mu}{AT^2}\right)^{1/2k-2}, \qquad p = y\frac{\mu}{T}\left(\frac{\mu}{AT^2}\right)^{1/2k-2} \tag{2.12}$$

removes all parameters so that (2.10) becomes

$$M: \begin{aligned} x_{n+1} &= x_n + y_n \\ y_{n+1} &= y_n - x_{n+1}^{2k-1}. \end{aligned} \tag{2.13}$$

The effect of increasing T (nonintegrability) is to move the point in x, y that represents q, p farther from the origin. The scaling fails when $k = 1$, that is, for the harmonic

oscillator ($V = \frac{1}{2}Aq^2$), and this case will be considered in detail in Section 8. The simplest nontrivial case is the quartic oscillator ($V = \frac{1}{4}Aq^4$) and this will be explored extensively in Section 10.

3. Mapping Wigner's Function

Since the structure of the classical map M is clearest in the phase plane, it is natural to study the quantum map $\hat{U}$ in the phase plane too. To achieve this, we work with Wigner's function [22], whose usefulness in semiclassical mechanics is now becoming apparent [8, 12, 13, 23–26, 42]. This is $W(q, p)$, defined for a state $\psi(q)$ by

$$W(q, p) \equiv \frac{1}{\pi\hbar} \int_{-\infty}^{\infty} dx\, e^{-2ipx/\hbar} \psi(q + x)\, \psi^*(q - x); \tag{3.1}$$

it has the useful properties that its projection along p is the coordinate probability density $|\psi(q)|^2$, and its projection along q is the momentum probability density. A straightforward calculation based on (2.9) shows that the quantum map transforming a Wigner function W_n into its iterate W_{n+1} is

$$W_{n+1}(q, p) = \int_{-\infty}^{\infty} dq' \int_{-\infty}^{\infty} dp'\, K(q, p; q', p')\, W_n(q', p'), \tag{3.2}$$

where the propagator K is

$$K(q, p; q', p') = \frac{2}{h} \delta\left(q' - q + \frac{p'T}{\mu}\right) \int_{-\infty}^{\infty} dx\, e^{(i/\hbar)[2x(p'-p) - T\{V(q+x) - V(q-x)\}]}. \tag{3.3}$$

This propagator represents an orthogonal operator since it follows on direct calculation that

$$\int_{-\infty}^{\infty} dq'' \int_{-\infty}^{\infty} dp''\, K(q, p; q'', p'')\, K(q', p'; q'', p'') = \delta(q - q')\, \delta(p - p'). \tag{3.4}$$

Moreover, our study of the classical limit in Section 4 shows the transformation to be proper. Thus, the propagator of Wigner's function has the single eigenvalue $+1$, and the eigenstates are Wigner functions which transform into themselves under (3.2), without a phase factor as in (2.3). These Wigner eigenstates can be more general than pure quantum eigenstates satisfying (2.3) since they can also represent a density matrix consisting of a mixture of pure eigenstates.

The Wigner propagator (3.3) transforms an old state in q', p' to a new state in q, p. Comparison with (2.10) shows that the coordinate part of this transformation occurs pointwise in conformity with the classical map M, while the momentum part is nonlocal and gives quantum spreading in the phase plane. The only exceptions are linear maps, for which the integral in (3.3) becomes a delta function so that the momentum maps classically too, as will be discussed in the next section.

For the quartic potential $V(q) = \frac{1}{4}Aq^4$, the propagator is

$$K(q, p; q', p') = \frac{2\delta(q' - q + p'T/\mu)}{\hbar^{2/3}(6ATq)^{1/3}} \operatorname{Ai}\left[\frac{-2(p' - p - TAq^3)}{\hbar^{2/3}(6ATq)^{1/3}}\right], \tag{3.5}$$

where Ai denotes the Airy function [27]. For small $\hbar$ the momentum part of this expression is concentrated near the zero of the argument of the Airy function, which occurs precisely at the classical p value given by M [Eq. (2.10)]; this result will now be generalized.

4. Semiclassical Theory: The Wigner Propagator

For small $\hbar$ the integrand in (3.3) is a rapidly oscillating function of x, and K can be approximated asymptotically by techniques employing stationary phase. The stationary points $x = x_0$ satisfy

$$p - p' = -\tfrac{1}{2}T[V'(q + x_0) + V'(q - x_0)], \tag{4.1}$$

which means that x_0 is chosen to make the average force at $q + x_0$ and $q - x_0$ drive the momentum from p' to p in the time T. If x_0 is a solution of (4.1), so is $-x_0$. Therefore, the stationary points occur in pairs; we consider explicitly only cases where there are two or none.

Graphically (Fig. 1), the mean force law implies that $q \pm x_0$ are the endpoints of that chord of the graph of the impulse $-TV'(q)$ whose midpoint lies at q, $p - p'$. The phase of the integrand in (3.3) at $x = \pm x_0$ is proportional to the area $\mathcal{A}(q, p - p')$, shown shaded on Fig. 1, between the chord and the curve. It is evident that as q, $p - p'$ approaches the curve of $-TV'(q)$ from its concave side, $\mathcal{A} \to 0$,

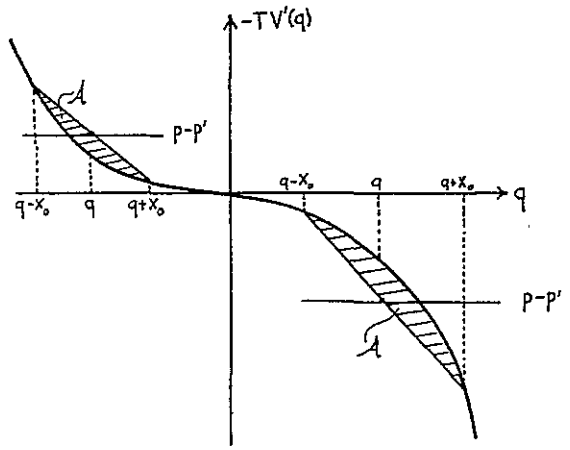

FIG. 1. Graphical interpretation of the semiclassical Wigner propagator (4.2), illustrating the chord construction, area rule, and sign convention for x_0, for two pairs of values of q, $p - p'$.

the two stationary points coalesce and $x_0 \to 0$. This is an important event because then q and $p - p'$ are related by M [Eq. (2.10)]. When stationary points coalesce, the simplest method of stationary phase becomes invalid and the more sophisticated technique of uniform approximation [28] must be employed, to give

$$K(q,p;q',p') = \frac{2}{\hbar^{2/3}}\left(\frac{2}{T}\right)^{1/2}\left[\frac{3\mathscr{A}(q,p-p')}{2}\right]^{1/6} \times \frac{\delta(q'-q+p'T/\mu)}{[V''(q+x_0)-V''(q-x_0]^{1/2}}\,\mathrm{Ai}\left[-\left\{\frac{3\mathscr{A}(q,p-p')}{2\hbar}\right\}^{2/3}\right]. \tag{4.2}$$

In this expression, $\mathscr{A}$ is chosen positive for points q, $p - p'$ on the concave side of the curve where the propagator is oscillatory, and the sign of x_0 is chosen (Fig. 1) so that the point $q + x_0$ has the algebraically smallest force gradient $-V''$. For points on the convex side of the curve, $\mathscr{A}$ is imaginary and the propatator, which decays exponentially, is then obtained by analytic continuation. The occurrence of Airy functions with maxima at where classical relations are satisfied, and the "chord" and "area" rules, are becoming familiar features of semiclassical mechanics in phase space [23–26].

For the quartic potential, (4.2) gives the exact propagator (3.5). Close to the classical curve, (4.2) gives the transitional approximation

$$K(q,p;q',p') = \frac{2\delta(q'-q+p'T/\mu)}{|\hbar^2TV'''(q)|^{1/3}}\,\mathrm{Ai}\left[\frac{2(p-p'+TV'(q))}{(-\hbar^2TV'''(q))^{1/3}}\right]. \tag{4.3}$$

The most important limit of (4.2), however, is the classical limit $\hbar = 0$, for which the relation

$$\lim_{\epsilon\to 0}\mathrm{Ai}(z/\epsilon)/\epsilon = \delta(z) \tag{4.4}$$

gives

$$K(q,p;q',p') = \delta(q'-q+p'T/\mu)\,\delta(p-p'+TV'(q)). \tag{4.5}$$

This is simply the classical Liouville propagator mapping q', p' to q, p by M.

The eigenfunctions of (4.5)—the classical limit of the Wigner eigenstates—are densities $W(q,p)$ on any region of the phase plane that is invariant under M. Such a region may be a fixed point of M (or a chain of m fixed points of M^m), or an invariant curve of M, or an area bounded by invariant curves (such an area could be an island entirely made up of invariant curves, or it could be a stochastic sea). We emphasize, however, that these classical eigenstates need not be the classical limits of Wigner functions representing quantum pure eigenstates. They may represent mixtures of eigenstates, or "quasi-modes" [29] that endure for long times (say of order $\hbar^{-1}$ or $e^{+1/\hbar}$) and then decay. In particular the existence of classical Wigner eigenstates located on unstable fixed points of M throws no light on the question of whether these fixed points (or, more generally, unstable closed classical orbits) can support quantum eigenstates. This is a controversial matter [10, 30] which will be studied in

a later paper [31] by investigating "Arnold's cat" [1], a totally ergodic map (all of whose fixed points are unstable). But it is valid to argue in the reverse direction and conclude that the classical limits of those Wigner functions that do represent pure quantum eigenstates must be eigenfunctions of (4.5) and, therefore, located on invariant manifolds of M. Some quantum eigenstates are located on quantized invariant curves of M; these will be discussed in Section 7. It is our opinion [12, 13] that other eigenstates are associated with whole stochastic regions rather than isolated unstable orbits since these regions are explored by typical orbits.

5. Semiclassical Theory: Iteration of States

Here we derive for quantum maps governed by the integral equation (2.9) an analog of time-dependent WKB theory [32] for the evolution of wavefunctions in conventional quantum mechanics. Let the wavefunction $\psi_n(q)$ at stage n be associated with a smooth curve $\mathscr{C}_n$ in the phase plane (Fig. 2), defined by

$$\mathscr{C}_n : p = p_n(q_n). \tag{5.1}$$

As is usual [25], we define ψ_n as

$$\psi_n(q) = a_n(q)\, e^{(i/\hbar)\int_{x_n}^{q} p_n(q_n)\,dq_n}, \tag{5.2}$$

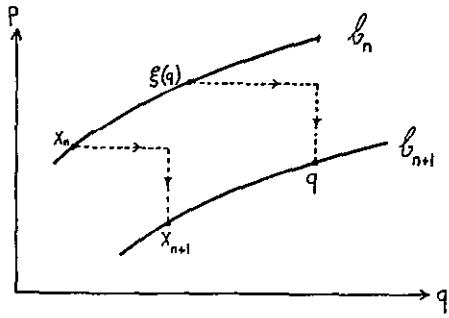

Fig. 2. Points and curves involved in semiclassical expressions for iteration of $\psi_n(q)$ to $\psi_{n+1}(q)$. Dashed lines denote classical trajectories.

where $a_n(q)$ is a smooth density along $\mathscr{C}$ and x_n an arbitrary constant phase reference level (Fig. 2). We now show that after a quantum mapping the new wave $\psi_{n+1}(q)$ can be written, apart from a phase factor, in a form identical to (5.2) but with all quantities referring to the classically mapped curve $\mathscr{C}_{n+1} = M\mathscr{C}_n$ (Fig. 2).

$\psi_{n+1}(q)$ is obtained by substituting (5.2) into the quantum map (2.9) and evaluating the integral (whose integrand oscillates rapidly when $\hbar$ is small) by stationary phase. To avoid confusion it is convenient to denote the integration variable by ξ rather than q'.

The phase of the integrand is then

$$\frac{1}{\hbar}\left[\frac{\mu(q-\xi)^2}{2T}+\int_{x_n}^{\xi} p_n(q_n)\,dq_n\right], \tag{5.3}$$

and is stationary at the point $\xi(q)$ satisfying

$$q=\xi(q)+(T/\mu)\,Pn(\xi(q)). \tag{5.4}$$

This equation may have many solutions, corresponding to multiple intersections of $\mathscr{C}_{n+1}$ with the line $q=$ const. We shall discuss this multivaluedness later; now we work out the contribution of a single root $\xi(q)$. By (2.10), $\xi(q)$ is the coordinate on $\mathscr{C}_n$ that maps onto q by M. Straightforward application of the method of stationary phase then gives

$$\psi_{n+1}(q)=a_{n+1}(q)\,e^{i(S_{n+1}(q)/\hbar)\mp\frac{1}{2}i\pi\pm\frac{1}{4}i\pi}, \tag{5.5}$$

where the action $S_{n+1}(q)$ is

$$S_{n+1}(q)=\int_{x_n}^{\xi(q)} p_n(q_n)\,dq_n+\frac{Tp_n^2(\xi(q))}{2\mu}-TV(q) \tag{5.6}$$

and

$$a_{n+1}(q)=a_n(\xi(q))\left|1+\frac{Tp_n'(\xi(q))}{\mu}\right|^{-1/2}, \tag{5.7}$$

and where the signs in (5.5) correspond to $1+Tp_n(\xi(q))/\mu \gtrless 0$.

To interpret the amplitude a_{n+1}, we note that, from (5.4), $1+Tp_n'/\mu$ equals the derivative $(d\xi/dq)^{-1}$. Thus

$$a_{n+1}(q)=a_n(\xi(q))\left|\frac{d\xi(q)}{dq}\right|^{1/2}, \tag{5.8}$$

showing that the intensity a_n^2 is obtained by pointwise convection from $\mathscr{C}_n$ to $\mathscr{C}_{n+1}$ followed by projection onto the q axis.

To interpret the phase, we first note that the contribution $-\frac{1}{2}\pi\pm\frac{1}{4}\pi$ in (5.5) distinguishes "proper" mappings, where $d\xi$ and dq have the same sign, from "improper" mappings, where $d\xi$ and dq have opposite sign. (The improper case could result from ξ and q lying on opposite side of turning points on their respective curves $\mathscr{C}_n$, and the resulting contribution $-\frac{1}{2}\pi$ is the well-known phase advance on passing through a caustic.)

Next, we transform the term $\int p_n\,dq_n$ in (5.6) in two stages. First, the integration variable q_n is changed to a coordinate q_{n+1} related to q_n by the first of the map equations (2.10) with p_n lying on $\mathscr{C}_n$. This gives

$$\int_{x_n}^{\xi(q)} p_n(q_n)\,dq_n = \int_{x_{n+1}}^{q} p_n(q_n)\,dq_{n+1} - \frac{T}{\mu}\int_{x_n}^{\xi(q)} p_n(q_n)\,p_n'(q_n)\,dq_n$$

$$= \int_{x_{n+1}}^{q} p_n(q_n)\,dq_{n+1} - \frac{Tp_n^2(\xi(q))}{2\mu} + \frac{Tp_n^2(x_n)}{2\mu}, \qquad (5.9)$$

where x_{n+1} is the iterate of x_n (Fig. 2). Then $p_n(q_n)$ is expressed in terms of the mapped momentum $p_{n+1}(q_{n+1})$ on $\mathscr{C}_{n+1}$ using the second of the map equations (2.10), giving

$$\int_{x_n}^{\xi(q)} p_n(q_n)\,dq_n = \int_{x_{n+1}}^{q} p_{n+1}(q_{n+1})\,dq_{n+1} + TV(q) - TV(x_{n+1})$$

$$- \frac{Tp_n^2(\xi(q))}{2\mu} + \frac{Tp_n^2(x_n)}{2\mu}. \qquad (5.10)$$

Thus (5.6) becomes

$$S_{n+1}(q) = \int_{x_{n+1}}^{q} p_{n+1}(q_{n+1})\,dq_{n+1} + \frac{Tp_n^2(x_n)}{2\mu} - TV(x_{n+1}). \qquad (5.11)$$

In terms of the continuous classical evalution between times nT and $(n+1)T$, governed by the Hamiltonian (2.6), $S_{n+1}(q)$ is given by the following formula, expected on general semiclassical grounds:

$$S_{n+1}(q) = \int_{nT}^{(n+1)T} L(q(t), \dot{q}(t), t)\,dt, \qquad (5.12)$$

where L denotes the Lagrangian function and $q(t)$ is any trajectory between x_n at $t = nT$ and q at $t = (n+1)T$. The expression (5.6) corresponds to the trajectory (Fig. 2) leading instantaneously from x_n to $\xi(q)$ along $\mathscr{C}_n$ and classically from $\xi(q)$ to q, while (5.11) corresponds to the trajectory leading classically from x_n to x_{n+1} and instantaneously from x_{n+1} to q along $\mathscr{C}_{n+1}$.

Combining (5.5), (5.8), and (5.11) we obtain the main result of this section, which is that the wave resulting from a semiclassical quantum map from $\psi_n(q)$ given by (5.2) is a sum of contributions

$$\psi_{n+1}(q) = a_n(\xi(q))\left|\frac{d\xi(q)}{dq}\right|^{1/2} e^{(i/\hbar)[\int_{x_{n+1}}^{q} p_{n+1}(q_{n+1})\,dq_{n+1} + Tp_n^2(x_n)/2\mu - TV(x_{n+1})]}$$

$$\times\, e^{-\frac{1}{2}i\pi\Theta(-\mathrm{sign}\,d\xi(q)/dq)} \qquad (5.13)$$

(where Θ denotes the unit step function), each contribution arising from one solution $\xi(q)$ of (5.4).

As n increases, it will generally be the case that $\mathscr{C}_n$ develops great complexity, whose structural elements, which we call whorls and tendrils, will be explored in the next section. Then there will be many intersections of $\mathscr{C}_{n+1}$ with the line $q = \text{const}$ (Fig. 3);

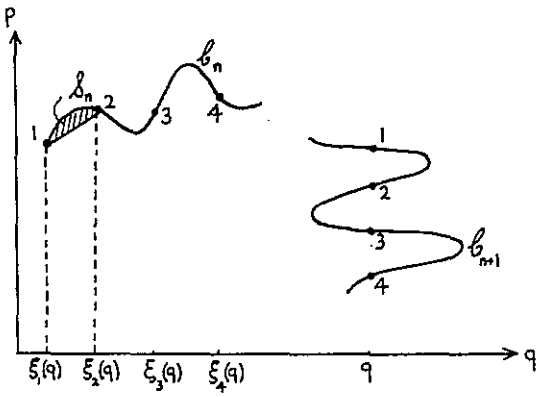

FIG. 3. A curve $\mathscr{C}_n$ whose iterate $\mathscr{C}_{n+1}$ generates four semiclassical contributions to $\psi_{n+1}(q)$. Areas $\mathscr{S}_n$ like that (shaded) between 1 and 2 must greatly exceed $\hbar$ if the method of stationary phase is to be valid.

the preimages on $\mathscr{C}_n$ of these intersections have the coordinates $\xi(q)$, giving stationary phase contributions (5.13) to ψ_{n+1}. For a given $\hbar$, however small, there will be an n for which these many stationary phase points ξ lie so close together that their action differences are not large in comparison with $\hbar$. Under these circumstances the stationary points are not well separated and the method of stationary phase breaks down. The wave is no longer given by the sum of terms like (5.13). There has been a transition to a new regime. Such transitions are expected quite generally [25] when the system's Hamiltonian depends on time, or when a wave based on a noninvariant curve evolves in a stationary Hamiltonian. One advantage of the map studied in this paper is that for it there exists a geometric criterion for the breakdown of the method of stationary phase, as will now be described.

Consider two neighboring coordinates ξ_1 and ξ_2 on $\mathscr{C}_n$ (Fig. 3) which map under M into points with the same q. The action difference ΔS_{n+1} of their contributions to ψ_{n+1} is, by (5.6),

$$\Delta S_{n+1} = \int_{\xi_1(q)}^{\xi_2(q)} p_n(q_n)\, dq_n + \frac{T}{2\mu}\,[p_n^2(\xi_2(q)) - p_n^2(\xi_1(q))]. \tag{5.14}$$

But the mapping law (5.4) shows that

$$\frac{T}{\mu}\,[p_n(\xi_2(q)) - p_n(\xi_1(q))] = -[\xi_2(q) - \xi_1(q)], \tag{5.15}$$

and so

$$\begin{aligned}\Delta S_{n+1} &= \int_{\xi_1(q)}^{\xi_2(q)} p_n(q_n)\, dq_n - \tfrac{1}{2}[p_n(\xi_2(q)) - p_n(\xi_1(q))][\xi_2(q) - \xi_1(q)] \\ &\equiv \mathscr{S}_n\,,\end{aligned} \tag{5.16}$$

where $\mathscr{S}_n$ is the area (shaded on Fig. 3) cut from $\mathscr{C}_n$ by the chord joining ξ_1, $p_n(\xi_1)$ and ξ_2, $p_n(\xi_2)$.

The method of stationary phase will be valid if

$$|\mathscr{S}_n| \gg \hbar \tag{5.17}$$

for all intersections $\xi(q)$. Isolated violations of this inequality, occurring near caustics [13] where the line $q = \text{const}$ is tangent to $\mathscr{C}_{n+1}$, can be dealt with by replacing the contribution (5.13) by a uniform approximation of Airy [28] or higher [33, 34] type. A global breakdown of stationary phase, leading to a transition to a wavefunction with different morphology, will occur if (5.17) is violated for most or all intersections. When this happens, most or all "convolutions" of $\mathscr{C}_n$, defined as regions between points on $\mathscr{C}_n$ whose images have the same q, have areas comparable with $\hbar$, and so it is not surprising that the quantum wave no longer discriminates the details of the classical curve.

The breakdown of formula (5.13) does not mean that all semiclassical methods must fail for large n. And indeed there does exist a method, employing Wigner's function, that appears to remain valid when $\psi_n(q)$ can no longer be resolved into individual contributions from intersections with $\mathscr{C}_n$. The method has already been described [13] and used to predict strikingly different morphologies for quantum wavefunctions corresponding to different sorts of classical motion, both for eigenstates [13] and evolving states [25]. The idea is to predict not all of the details of the wave function but the probability density $|\psi_n(q)|^2$, smoothed over a de Broglie wavelength (and also the pattern of oscillations of $\psi_n(q)$ as embodied in its autocorrelation function [13]).

To achieve this, the classical Wigner function corresponding to $\psi_n(q)$ is constructed, as follows: let the initial curve $\mathscr{C}_0$ be

$$\mathscr{C}_0 : f(X) = 0, \tag{5.18}$$

so that

$$[W_0(q, p)]_{\text{classical}} = \delta[f(X)], \tag{5.19}$$

where X denotes q, p and $f(X)$ is chosen to give W_0 the correct density round $\mathscr{C}_0$. Then using the Liouville propagator (4.5) gives

$$[W_n(q, p)]_{\text{classical}} = \delta[f(M^{-n}X)]. \tag{5.20}$$

The classical probability density is then

$$|\psi_n(q)|^2_{\text{classical}} = \int_{-\infty}^{\infty} dp\, \delta[f(M^{-n}X)]. \tag{5.21}$$

Since $[W_n(q, p)]_{\text{classical}}$ is a delta function on $\mathscr{C}_n$, this integral over p consists of discrete contributions from intersections of $\mathscr{C}_n$ with $q = \text{const}$. When $\mathscr{C}_n$ is compli-

cated there will be many intersections, and $|\psi_n(q)|^2_{\text{classical}}$ will be a very spiky function, with many caustic divergences at q values where the tangent to $\mathscr{C}_n$ points in the p direction. This will be illustrated by computation in Section 10.

The crucial final step is to perform a local smoothing of $|\psi_n(q_n)|^2_{\text{classical}}$ over a typical de Broglie wavelength at q, that is, over a distance h/p where p is the momentum of a typical intersection of $\mathscr{C}_n$ with the line $q = \text{const}$. The result appears to be a close approximation to the exact quantum probability density $|\psi_n(q)|^2$, smoothed in the same way, even when $\mathscr{C}_n$ gets very complicated, as will be evident from computations presented in Section 10.

We cannot provide a formal basis for this procedure, but its justification probably runs along the following lines: The exact Wigner function $W_n(q, p)$ is related to the unsmoothed classical Wigner function (5.20) by quantum spreading. This spreading is now well understood for pretransition states, where $\mathscr{C}_n$ is not highly convoluted: it takes the form of Airy fringes [24–26] decorating $\mathscr{C}_n$ and softening the delta function in (5.20). After the transition, the spreading, whose details are unknown, must surely be the result of interference among convolutions extending over areas $\hbar$. By performing the local smoothing over $|\psi_n(q)|^2_{\text{classical}}$ we average away this structure that we do not understand.

Admittedly this procedure is crude, but it does preserve features of the wave since it predicts the following difference between pretransition and postransition probability densities $|\psi_n|^2$, well borne out by the numerical experiments in Section 10: The smoothed pretransition $|\psi_n|^2$ is dominated by a few caustics, whose divergence is softened but which still give rise to peaks. The smoothed posttransition $|\psi_n|^2$ is not dominated by individual caustics since these are now thickly clustered and separated by less than the quantum smoothing distance, so that they can no longer be resolved after smoothing. At the risk of laboring this point, we put it another way, which illustrates a general principle: The smoothing is on a scale $\hbar$. Before the transition, its main effect is to blur quantum oscillatory detail and leave a mostly smooth classical background. After the transition, its main effect is to blur and amalgamate classical caustic singularities, leaving a probability density with structure on all scales down to $\hbar$. The general principle is that $\hbar$ has fundamentally different effects on classically smooth and classically chaotic systems.

6. Whorls and Tendrils

Considering the vast effort that has been spent studying the orbits of points under M, it is surprising that nobody seems to have studied the changing forms of curves under M and classified their convolutions into different types. Here we make a first attempt to do this, motivated by the obvious relevance to evolving quantum states.

$\mathscr{C}_n$ becomes complicated because M has fixed points. To see this, consider an initial curve passing through several fixed points. When iterated by M, $\mathscr{C}_n$ is pinned at these points but is otherwise free to evolve. Now points on $\mathscr{C}_0$ that are not fixed will map over distances increasing with n (either simple or complex bounded circuits, or escape

to infinity). Therefore, it is almost inevitable that $\mathscr{C}_n$ will become more and more convoluted, its length increasing while its area remains the same. The only exceptions to this are invariant curves of M (or of M^n where n is finite), whose points map onto one another rather than exploring fresh territory, and curves under linear maps M, which rotate rigidly if M is elliptic [1, 4] and stretch to a fixed straight line if M is hyperbolic. Since M is a continuous map, the evolution of curves passing near but not through fixed points will be qualitatively similar: $\mathscr{C}_n$ will still convolute as n increases.

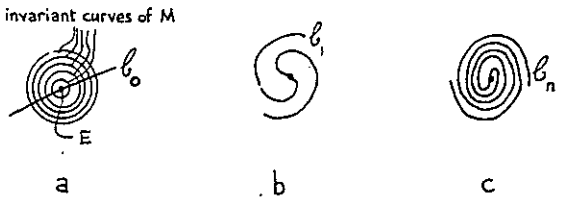

FIG. 4. Development of a whorl from a curve $\mathscr{C}_0$ passing through an elliptic fixed point E surrounded by invariant curves of M whose rotation numbers increase away from E.

Consider first the case where $\mathscr{C}_0$ passes through an elliptic fixed point E of M (Fig. 4a). Generically E will be surrounded by invariant curves of M filling an "island" of finite area. Each such curve is characterized by its rotation number r, which varies smoothly from curve to curve across the island. (For any invariant curve $\mathscr{C}$, r is defined as the average, over infinitely many iterations of M, of $1/2\pi$ times the angle swept out during a single iteration by the radius vector joining a point X on $\mathscr{C}$ to any fixed point inside $\mathscr{C}$. The angle can always be defined so that $0 \leqslant r < 1$.) Each point on $\mathscr{C}_0$ maps round E along one of the invariant curves at a rate determined by r. Different points rotate at different rates (Fig. 4b), so the upshot is that $\mathscr{C}_n$ gets tightly wrapped round E (Fig. 4c) and eventually fills the island. We call this spiral curve a "whorl." (For an early example, see [43].)

We shall also use the term whorl for the "spiral galaxy" generated when $\mathscr{C}_0$ is closed and surrounds E without being one of the invariant curves. This structure, which again originates in differing rotation numbers, will be illustrated in Section 10. Its end result $\mathscr{C}_\infty$ fills a region R of the phase plane bounded by the invariant curves touched by $\mathscr{C}_0$. As discussed elsewhere [25] this filling is not uniform but rises to infinity on the boundary of R, projecting to give characteristic singularities of $|\psi_\infty(q)|^2_{\text{classical}}$ different from those at caustics.

Now consider the case where $\mathscr{C}_0$ passes through a hyperbolic fixed point H of M (Fig. 5a). H is unstable, and the generic situation is for points near H to map chaotically throughout a region of the phase plane. The origin of this behavior [1–4] is in the infinitely numerous "homoclinic points" which are intersections of the "ingoing" and "outgoing" curves H_- and H_+ (Fig. 5a), made up respectively of points that will map into H as $n \to \infty$ and points that mapped out of H at $n \approx -\infty$. Provided the initial curve $\mathscr{C}_0$ does not coincide with H_-, it will when iterated rotate

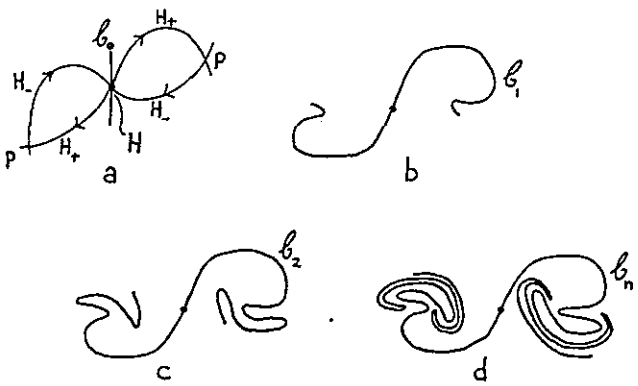

FIG. 5. Growth of tendrils on the iterates of a curve $\mathscr{C}_0$ passing through a hyperbolic fixed point H whose ingoing and outgoing curves H_- and H_+ cross at homoclinic points P (only the first of which are shown).

towards H_+ and stretch exponentially fast along it. Now H_+ is complicated: it swings back and forth across H_- (between homoclinic points) ever more violently, its convolutions becoming thinner and longer. As n increases (Figs. 5b–d), $\mathscr{C}_n$ snakes its way along H_+ and shares its complication. We describe this by saying that $\mathscr{C}_n$ grows "tendrils." Eventually $\mathscr{C}_n$ explores the whole of the unstable region. This may be finite (between two invariant curves) or infinite (points escape to infinity under M). In the former case, the ultimate classical probability density $|\psi_\infty(q)|^2_{\text{classical}}$ terminates on "anticaustics" [13] at the boundaries of the projection of $\mathscr{C}_\infty$. In the latter case, $|\psi_n(q)|^2_{\text{classical}}$ spreads all along the q axis as $n \to \infty$.

Whorls and tendrils are the structural elements of $\mathscr{C}_n$'s developing complication. A typical $\mathscr{C}_0$ may pass close to several elliptic and hyperbolic fixed points of M, and will therefore evolve into a fantastic shape incorporating both whorls and tendrils. One such shape is sketched in Fig. 6 for a simple "ideal" case. Its curlings and flailings are reminiscent of cream spreading on coffee, and suggests that the study of generic area-preserving maps of curves on a plane, or surfaces in space, might be a profitable way to study turbulent mixing (the very genericity of this behavior makes

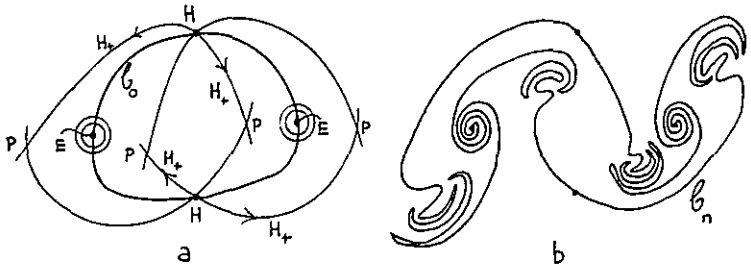

FIG. 6. (a) Initial curve $\mathscr{C}_0$ passing through elliptic (E) and hyperbolic (H) fixed points of M; outgoing curves H_+ and the first homoclinic points P are marked. (b) The two whorls and four groups of tendrils on the iterated curve $\mathscr{C}_n$.

turbulence seem "almost" inevitable; what needs to be explained is nonturbulent flow).

There is ample algebraic opportunity for the rapid development of complexity in $\mathscr{C}_n$. Consider the standard polynomial maps (2.13) generated by the potential (2.11), and let $\mathscr{C}_0$ be a contour of the average potnetial $\bar{H}$, namely,

$$\frac{y^2}{2} + \frac{x^{2k}}{2k} = C, \tag{6.1}$$

where C is a constant. This is a curve of degree $2k$. Under (2.13), $\mathscr{C}_0$ iterates to $\mathscr{C}_n$, whose degree is $2k \times (2k-1)^n$. So for the simplest nontrivial case of the quartic map ($k = 2$) the degrees of $\mathscr{C}_0$, $\mathscr{C}_1$, $\mathscr{C}_2$, and $\mathscr{C}_3$ are 4, 12, 36, and 108! This accounts for the complexity of the curve maps to be shown in Section 10.

A measure of the increasing complexity of $\mathscr{C}_n$ is its increasing length $\mathscr{L}_n$. For whorls, the stable linear rotation around elliptic fixed points implies

$$\mathscr{L}_n \sim An \qquad \text{as} \quad n \to \infty, \tag{6.2}$$

where A is constant. For tendrils, the unstable exponential stretching away from hyperbolic fixed points implies

$$\mathscr{L}_n \sim Be^{Cn} \qquad \text{as} \quad n \to \infty, \tag{6.3}$$

where B and C are constant.

We can use these measures of complexity to get estimates of the iteration numbers n_t near which the wave $\psi_n(q)$ undergoes the transition discussed in the last section and ceases to be given by a sum of semiclassical waves (5.13). This occurs when typical convolutions (as defined in Section 5) have areas of order $\hbar$. Since the total area of $\mathscr{C}_n$ is preserved under M,areas of individual filamentary convolutions might be proportional to $\mathscr{L}_n^{-1}$. It would then follow that

$$\begin{aligned} n_t &\propto \hbar^{-1} \qquad \text{(whorls)}, \\ n_t &\propto \ln(\hbar^{-1}) \qquad \text{(tendrils)}. \end{aligned} \tag{6.4}$$

Thus the transition of ψ_n associated with tendrils (quantum stochasticity) should occur much sooner than that associated with whorls.

7. Semiclassical Theory: Eigenstates

Our main concern in this section will be with the stationary states of the quantum map, that is, with the eigenfunctions and eigenvalues of $\hat{U}$. First, however, we deal briefly with a more general aspect of quantization that has nothing to do with dynamics but concerns any state $\psi(q)$ associated with a smooth simple closed curve $\mathscr{C}$ in the

phase plane. Semiclassically, any such state can be written as the sum of waves of the form (5.2), each contribution arising from an intersection of $\mathscr{C}$ with the line $q = \text{const}$. These contributions are connected by caustics, where (5.2) breaks down. Now $\psi(q)$ must be single valued, and so must return to its original value after a circuit of $\mathscr{C}$ with proper analytic continuation through caustics.

Standard WKB arguments requiring analyticity in the complex q plane [35], or the simultaneous validity of (5.2) and its momentum-axis analog [7, 9], or that the semiclassical Wigner function be single valued [24], show that $\psi(q)$ can be single valued only if the area of $\mathscr{C}$ is quantized according to

$$I \equiv (1/2\pi) \int p(q)\, dq = (k + \tfrac{1}{2})\hbar \qquad (k = 0, 1, 2, \ldots). \tag{7.1}$$

This result is valid for a simple closed curve $\mathscr{C}$ of any shape provided it is sufficiently smooth.

Now we study the stationary states of the quantum map, defined by (2.3). Their wavefunctions $\phi(q)$ must iterate into themselves, apart from the phase factor $-\alpha/\hbar$, by the integral equation (2.9). We restrict ourselves to eigenfunctions associated with smooth closed curves $\mathscr{C}$. These iterate semiclassically according to (5.13). Obviously $\phi(q)$ can be a stationary state only if $\mathscr{C}$ is an invariant curve of M, quantized by (7.1).

To find the wavefunction for this state, we need consider only one branch $p(q)$ of $\mathscr{C}$, whose contribution to ϕ is given by (5.2) without the suffixes n. This formula involves the phase reference level x; we shall require the coordinate of the iterate of the point $(x, p(x))$, which we denote by $x_1(x)$. Then according to (5.13) ϕ iterates to

$$\langle q \mid \hat{U} \mid \phi \rangle = \phi(q) \frac{a(\xi(q))}{a(q)} \left| \frac{d\xi(q)}{dq} \right|^{1/2} e^{(i/\hbar)[-\int_x^{x_1(x)} p(q)\,dq + Tp^2(x)/2\mu - TV(x_1(x))]}, \tag{7.2}$$

where, as in Section 5, $\xi(q)$ is the coordinate of the point that iterates to $(q, p(q))$. Stationarity requires

$$a(q) = a(\xi(q)) \left| \frac{d\xi(q)}{dq} \right|^{1/2}. \tag{7.3}$$

This equation has the solution

$$a(q) = (\text{const}) \left| \frac{d\theta(q)}{dq} \right|^{1/2}, \tag{7.4}$$

where $\theta(q)$ is an M-invariant measure on $\mathscr{C}$, which provided it exists is easily constructed to any desired accuracy by repeated mappings round $\mathscr{C}$ (for an integrable map, θ is the "angle" variable conjugate to the action).

Having found the stationary state, we can write down its eigenvalue α [Eq. (2.3)] from the phase in (7.2). It is

$$\alpha = \int_x^{x_1(x)} p(q)\, dq - \frac{Tp^2(x)}{2\mu} + TV(x_1(x)). \tag{7.5}$$

The dependence on x is illusory since

$$\frac{d\alpha}{dx} = p(x_1(x))\frac{dx_1(x)}{dx} - p(x) - \frac{Tp(x)}{\mu} - TV'(x_1(x))\frac{dx_1(x)}{dx} = 0, \tag{7.6}$$

as follows from the map equations (2.10).

An alternative and physically more transparent expression for α, which is valid not only for the maps considered here but for any map generated by a Hamiltonian with period T, can be derived from the Lagrangian formula (5.12), or directly from (7.5). It involves the changing momentum $p(x, t)$ on the curve that maps away from and back to $\mathscr{C}$ as t varies from nT to $(n + 1)T$. The expression is

$$\alpha = \int_0^T dt\, H(x, p(x, t), t) = T\bar{E}, \tag{7.7}$$

where $\bar{E}$ is the average energy on $\mathscr{C}$ over a period at the coordinate x. This result justifies the expression "quasi-energy" [36] for α/T. (The independence of α from x follows easily from Hamilton's equations and the time periodicity of $p(x, t)$.)

Both (7.5) and (7.7) have the awkward feature of appearing to depend on x. To obtain an expression for α that manifestly involves only the goemetry of $\mathscr{C}$ and contains no reference to any particular point on $\mathscr{C}$, we average over all iterations of $(x, p(x))$ and use the fact that these iterations will eventually cover $\mathscr{C}$. In an obvious notation,

$$\alpha = \lim_{N\to\infty} \frac{1}{N} \sum_{n=1}^{N} \int_{q_n}^{q_{n+1}} p(q)\, dq - \frac{T\overline{p_n^2}}{2\mu} + T\overline{V(q_n)}. \tag{7.8}$$

The first term involves successive areas on $\mathscr{C}$ that fit together to cover $\mathscr{C}$ repeatedly. They give

$$\lim_{N\to\infty} \frac{1}{N} \sum_{n=1}^{N} \int_{q_n}^{q_{n+1}} p(q)\, dq = r \oint p(q)\, dq, \tag{7.9}$$

where r is the rotation number of $\mathscr{C}$.

The second term in (7.8) can be rewritten using an amusing map analog of the virial theorem, which follows from (2.10):

$$\begin{aligned} \tfrac{1}{2}T\overline{p_n^2}/\mu &= \tfrac{1}{2}T\overline{V'(q_{n+1})\, q_{n+1}} - \tfrac{1}{2}\overline{q_n p_n} + \tfrac{1}{2}\overline{p_1 q_1} \\ &= \tfrac{1}{2}T\overline{V'(q_{n+1})\, q_{n+1}}\,. \end{aligned} \tag{7.10}$$

Therefore the eigenvalue α becomes

$$\alpha = r \oint p(q)\, dq - \frac{T}{2}\overline{q^3 \frac{d[V(q)/q^2]}{dq}}, \tag{7.11}$$

where the average is over all iterations of q round $\mathscr{C}$. For the standard maps (2.11) this simplifies to

$$\alpha = r \oint p(q)\, dq - T(k - 1)\,\overline{V(q)}, \tag{7.12}$$

a formula that will be employed in the next section for the discrete oscillator map $k = 1$.

In the integrable limit $T \to 0$, all these formulae for α reduce to $T\bar{H}(q, p)$, as is obvious from (7.7) and the fact that $\mathscr{C}$ is a contour of H when $T = 0$. From (7.11) we get in this way an interesting formula for the energy E of motion under $\bar{H}(q, p)$. The rotation number is

$$r = T/\tau \tag{7.13}$$

where τ is the period of motion round $\mathscr{C}$. Then (7.11) gives

$$E = \frac{1}{\tau}\left\{\oint p(q)\,dq - \int_0^\tau dt\, q^3(t)\,\frac{\partial[V(q)/q^2]_{q=q(t)}}{\partial q}\right\}. \tag{7.14}$$

Now we study eigenstates associated with a chain of m islands (Fig. 7) surrounding elliptic fixed points of M^m. Each invariant curve $\mathscr{C}$ of M now consists of m separate closed loops, denoted by $\mathscr{C}_j$ $(1 \leqslant j \leqslant m)$, all with the same area. Each $\mathscr{C}_j$ is an invariant curve of M^m, and maps onto $\mathscr{C}_{j+1}$ under M.

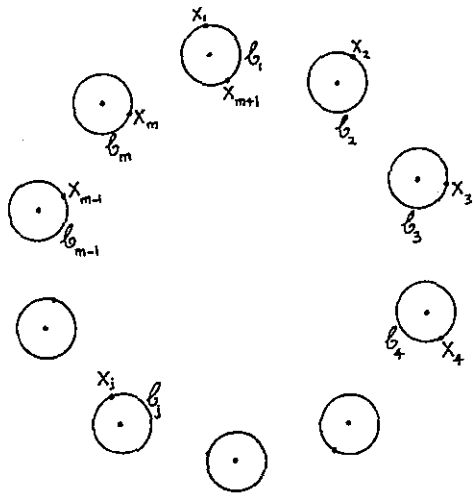

FIG. 7. Invariant curves $\mathscr{C}_1, \ldots, \mathscr{C}_m$ on a chain of m islands centered on elliptic fixed points of M^m. The points $x_2, \ldots, x_{m+1}$ are the first m iterates of x_1.

The eigenfunctions $\phi(q)$ are made up of m separate pieces $\phi_j(q)$ localized on $\mathscr{C}_j$. Single valuedness of each piece implies that the area of each $\mathscr{C}_j$ is quantized by (7.1). For each branch of $\phi_j(q)$ we take a semiclassical wave of the form (5.2). The phase reference levels are taken as x^j, where x_1 is the coordinate of a point on $\mathscr{C}_1$ (Fig. 7) and $x_2, \ldots, x_m$ are its iterates on $\mathscr{C}_2, \ldots, \mathscr{C}_m$. We shall also require the mth iterate

x_{m+1}, which again lies on $\mathscr{C}_1$ and is generally different from x_1. Combining these waves with phases $\mu_j/\hbar$ gives

$$\phi(q) = \sum_{j=1}^{m} \phi_j(q)\, e^{i\mu_j/\hbar} = \sum_{j=1}^{m} a_j(q)\, e^{(i/\hbar)\int_{x_j}^{q} p_j(q')\,dq' + i\mu_j/\hbar}. \tag{7.15}$$

The eigenvalue α of this island-chain eigenstate (and also the constants μ_j) are determined by iteration using (5.13). This gives

$$\begin{aligned}\langle q \mid \hat{U} \mid \phi\rangle = &\sum_{j=1}^{m-1} \phi_{j+1}(q)\, e^{(i/\hbar)(\mu_j - Tp_j^2(x_j)/2\mu - TV(x_{j+1}))} \\ &+ \phi_1(q)\, e^{(i/\hbar)(\mu_m + Tp_m^2(x_m)/2\mu - TV(x_{m+1}) - \int_{x_1}^{x_{m+1}} p_1(q)\,dq)},\end{aligned} \tag{7.16}$$

where the different form of the last term arises from the mismatch of x_1 and x_{m+1} on $\mathscr{C}_1$. Comparison with (7.15) and use of (2.3) shows that ϕ is an eigenfunction if

$$\begin{aligned}\mu_1 - \alpha &= \mu_m + Tp_m^2(x_m)/2\mu - TV(x_{m+1}) - \int_{x_1}^{x_{m+1}} p_1(q)\,dq, \\ \mu_2 - \alpha &= \mu_1 + Tp_1^2(x_1)/2\mu - TV(x_2), \\ &\vdots \\ \mu_m - \alpha &= \mu_{m-1} + Tp_{m-1}^2(x_{m-1})/2\mu - TV(x_m).\end{aligned} \tag{7.17}$$

The μ_j cancel on adding these equations, and so the eigenvalue α is

$$\alpha = \frac{T}{m} \sum_{j=1}^{m} \left[V(x_{m+1}) - \frac{p_m^2(x_m)}{2\mu} \right] + \frac{1}{m} \int_{x_1}^{x_{m+1}} p_1(q)\,dq. \tag{7.18}$$

Despite appearances, this α, like (7.5) is independent of the choice of starting position x_1, and it is also independent of the choice of starting island. Again this invariance can be made manifest by averaging, this time over the iterations $x_{m+1}, x_{2m+1}, \ldots$ of x_1. The result is a formula for α identical with (7.11), where $\oint p\,dq$ is the area of a single island and where r is the effective rotation number of M, that is, of a point jumping from island to island, and not the rotation number mr of M^m (generated by successive returns to the same island).

We have considered only eigenstates associated with smooth closed curves $\mathscr{C}$. If $\mathscr{C}$ is too irregular in the sense that its convolutions (as defined in Section 5) do not have areas large in comparison with $\hbar$, then eigenfunctions based on (5.2) do not exist because the iteration formula (5.13) is no longer valid and such functions do not map onto themselves. The extreme case is a bounded stochastic region of the phase plane, which can be thought of as an infinitely convoluted invariant curve filling an area. It is then possible to conjecture the form of the eigenfunctions [13], but we do not know what quantization rule replaces (7.1) (for suggestions see [10, 40]), or what eigenvalue formula replaces (7.5), (7.7), or (7.11) (of these three, (7.7) seems most amenable to generalization).

8. Exact Solution for Discrete Harmonic Oscillator Quantum Maps

We seek eigenstates $\phi_k(q)$ of the integral equation (2.9) in the parabolic potential well

$$V(q) = \tfrac{1}{2}\mu\omega^2 q^2. \tag{8.1}$$

Changing to new variables

$$\begin{aligned} x &\equiv (\mu\omega/\hbar)^{1/2}\, q, \qquad \tau \equiv \omega T \\ \phi_k(q) &\equiv u_k(x) \end{aligned} \tag{8.2}$$

gives

$$e^{\frac{1}{2}i\tau x^2} e^{-i\alpha_k/\hbar} u_k(x) = \frac{e^{-i\pi/4}}{(2\pi\tau)^{1/2}} \int_{-\infty}^{\infty} dx'\, u_k(x')\, e^{i(x-x')^2/2\tau} \tag{8.3}$$

to be solved for the eigenfunctions $u_k(x)$ and eigenvalues α_k.

By analogy with the continuous case ($\tau \to 0$) we use the ansatz

$$u_k(x) = H_k(\sigma' x)\, e^{-\frac{1}{2}\sigma^2 x^2}, \tag{8.4}$$

where H_k denotes the kth Hermite polynomial. After some algebra and use of the standard integral

$$\int_{-\infty}^{\infty} dz\, H_k(az)\, e^{-(z-b)^2} = \pi^{1/2}(1 - a^2)^{k/2}\, H_k\left(\frac{ab}{(1-a^2)^{1/2}}\right), \tag{8.5}$$

(8.3) becomes

$$\begin{aligned} &e^{\frac{1}{2}i\tau x^2} e^{-\frac{1}{2}\sigma^2 x^2} H_k(\sigma' x)\, e^{-i\alpha_k/\hbar} \\ &= \left\{\frac{[1 + i\tau(\sigma^2 - 2\sigma'^2]^{k/2}}{(1 + i\tau\sigma^2)^{(k+1)/2}}\right\} e^{-x^2\sigma^2/2(1+i\tau\sigma^2)} H_k\left\{\frac{\sigma' x}{(1 + i\tau\sigma^2)\left(1 - \dfrac{2i\tau\sigma'^2}{1 + i\tau\sigma^2}\right)^{1/2}}\right\}. \end{aligned} \tag{8.6}$$

The coefficients of x^2 in the exponentials must match, and this leads to

$$\sigma^2 = (1 - \tfrac{1}{4}\tau^2)^{1/2} + \tfrac{1}{2}i\tau. \tag{8.7}$$

To ensure a square-integrable wave function the positive square root must be taken. The same condition implies that $\tau = \omega T < 2$, whose classical meaning will soon become apparent. Note that $|\sigma| = 1$.

The arguments of the Hermite polynomials must match, and this gives

$$\sigma' = (1 - \tfrac{1}{4}\tau^2)^{1/4}. \tag{8.8}$$

With these values of σ and σ' the first factor on the r.h.s. of (8.6) is σ^{-4k-2}, which has unit modulus and leads to identification of the eigenvalues as

$$\alpha_k = 2(k + \tfrac{1}{2})\,\hbar \arcsin \tfrac{1}{2}\omega T. \tag{8.9}$$

In the continuum limit $T \to 0$ this gives $\alpha_k = (k + \frac{1}{2})\,\hbar\omega T$ which as expected are just the ordinary harmonic oscillator levels multiplied by T. The effect of the discretizing perturbation T is to increase the level spacings by a factor that rises to $\frac{1}{2}\pi$ in the limiting case $\omega T = 2$.

It is interesting to note that the eigenfunctions (8.4) and the eigenvalues (8.9) are generated by the following time-independent Hamiltonian operator $\hat{H}$:

$$\hat{H} = \frac{\arcsin \frac{1}{2}\omega T}{\frac{1}{2}\omega T}\, e^{-im\omega^2\hat{q}^2T/4\hbar} \left\{ \frac{\hat{p}^2}{2\mu(1 - \frac{1}{4}\omega^2T^2)^{1/2}} + \frac{\mu\omega^2\hat{q}^2}{2}\left(1 - \frac{1}{4}\omega^2T^2\right)^{1/2} \right\} e^{im\omega^2\hat{q}^2T/4\hbar}. \tag{8.10}$$

This is $i\hbar/T$ times the logarithm of $\hat{U}$ given by Eq. (2.7) with the potential (8.1). All quantum maps $\hat{U}$ can be alternatively considered in terms of some effective Hamiltonian, but for nonquadratic potentials $\hat{H}$ is intractably complicated and would not generate any simple differential equation for the eigenfunctions.

The classical mechanics of the discrete harmonic oscillator is based on the map (2.10). For the potential (8.1) this is linear, with matrix

$$M = \begin{pmatrix} 1 & T/\mu \\ -\mu\omega^2 T & 1 - \omega^2T^2 \end{pmatrix}. \tag{8.11}$$

The eigenvalues of M are

$$\lambda = +1 - \tfrac{1}{2}\omega^2T^2 \pm i\omega T(1 - \tfrac{1}{4}\omega^2T^2)^{1/2}. \tag{8.12}$$

When $\omega T < 2$ these are complex conjugates, showing that M is a stable map [1, 4]. Points iterate round ellipses, with rotation number

$$r = \frac{1}{2\pi}\arg\lambda = \frac{1}{2\pi}\arcsin\left[\omega T\left(1 - \frac{\omega^2T^2}{4}\right)^{1/2}\right] = \frac{1}{\pi}\arcsin\frac{\omega T}{2}. \tag{8.13}$$

This result can be used as a test of the semiclassical eigenvalue formula (7.12). Since $k = 1$ for quadratic potentials, only the term $r\oint p\,dq$ contributes to α. The phase integral is quantized by (7.1), so (8.13) gives eigenvalues in precise agreement with the exact equation (8.9).

When $\omega T > 2$ the eigenvalues are real and negative. This shows M to be unstable, with a hyperbolic fixed point with reflection [1, 4] at the origin. Points iterate to infinity by jumping between members of a pair of hyperbolae. This classical instability, induced by the perturbation T, accounts for the absence of quantum eigenfunctions when $\omega T > 2$.

9. Exact Solution for Gaussian Packets in Discrete Parabolic-Potential Quantum Maps

In this section we again consider a parabolic poetntial, which we now write as

$$V(q) = \frac{S\mu q^2}{2T^2}, \tag{9.1}$$

where the strength S is analogous to our previous $\omega^2 T^2$. However, we shall allow S to be negative, in which case the classical map M is unstable, with an ordinary hyperbolic fixed point at the origin. The results of Section 8 showed that M is stable if $0 < S < 4$ and unstable with reflection if $S > 4$.

The question we answer here is: what happens to Gaussian wave packets under the quantum map generated by (9.1)? In a convenient notation, such a packet has the wavefunction

$$\psi_n(q) = C_n e^{i w_n \mu (q-q_n)^2/2\hbar T}. \tag{9.2}$$

w_n denotes the dimensionless complex width of the packet, and q_n its complex centre. For a normalizable packet, Im $w_n > 0$. Under iteration by (2.9) this packet remains Gaussian and preserves its normalization. Some algebra shows that w_n and q_n iterate according to the mappings

$$w_{n+1} = \frac{w_n}{1 + w_n} - S, \tag{9.3}$$

and

$$q_{n+1} = q_n/[1 - S(1 - w_n^{-1})]. \tag{9.4}$$

We study only the evolution of w_n.

Gaussians whose width w^* does not change correspond to fixed points of (9.3). These are

$$w_{\pm}^* = -\tfrac{1}{2}[S \pm (S^2 - 4S)^{1/2}]. \tag{9.5}$$

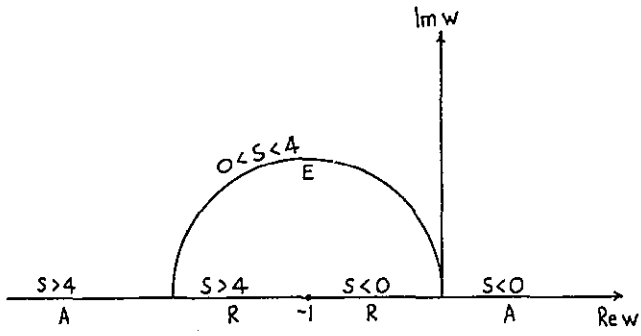

FIG. 8. Location of fixed points in the plane of complex Gaussian wave packet widths w, for different regimes of potential strength S. The stability type of the fixed points is as indicated; A means attractor, R means repeller, and E means elliptic stable.

For $0 < S < 4$ these fixed points are complex conjugates on the unit circle (Fig. 8) centered on -1 (i.e., $|1 + w_{\pm}|^2 = 1$). The $+i$ root must be taken, and the Gaussians then correspond to the ground-state oscillator functions considered previously, with width given by (8.7). For $S < 0$, w_+^* lies on the positive real axis and w_-^* on the negative real axis between -1 and 0. For $S > 4$, w_+^* lies on the negative real axis between -2 and -1, and w_-^* lies on the negative real axis between $-\infty$ and -2.

To investigate the stability of these unchanging Gaussians we study wave packets close to w^*, that is, for which

$$\delta_n \equiv w_n - w^* \tag{9.6}$$

is small. Then it is permissible to linearize (9.3) in δ_n to give

$$\delta_{n+1} = \delta_n/(1 + w^*)^2. \tag{9.7}$$

Thus w^* is an attractor (A) if $|1 + w^*| > 1$, a repeller (R) if $|1 + w^*| < 1$, and elliptic stable (E) if $|1 + w^*| = 1$. These stability domains are marked on Fig. 8.

The global flow of Gaussians in the w plane can be studied with the aid of the following exact solution of (9.3):

$$w_n = \frac{w^*(1 + w^*)^{2n}(w_0 - w^* - (S^2 - 4S)^{1/2}) - (w_0 - w^*)(w^* - (S^2 - 4S)^{1/2})}{(1 + w^*)^{2n}(w_0 - w^* - (S^2 - 4S)^{1/2}) + (w_0 - w^*)}, \tag{9.8}$$

where w^* can denote w_+^* or w_-^* provided $(S^2 - 4S)^{1/2}$ is taken with the corresponding sign. This result confirms the correctness of the stability analysis. For $0 < S < 4$, w_n iterates round a closed curve surrounding w_+^* or w_-^*; these curves are topologically like the equipotentials between equal positive charges on w_+^* and w_-^*. For $S < 0$ or $S > 0$, w_n iterates along curves connecting a repeller within the unit circle centred on -1 with an attractor outside this circle; the curves are topologically like lines of force between a negative charge at w_-^* and a positive charge at w_+^*.

These results describe in detail how Gaussians oscillate in width around the ground state described in Section 8, or spread indefinitely along the q axis, according to whether or not S lies between 0 and 4.

The continuum limit $T \to 0$ corresponds, from (9.1), to $S \to 0$. Then Gaussians oscillate in width if $S > 0$ (particle in a parabolic well) or spread if $S < 0$ (particle scattered from parabolic barrier), as expected.

10. Computations for Discrete Quartic Oscillator

In this section we shall iterate curves and wavefunctions under the map generated by

$$V(q) = \tfrac{1}{4}Aq^4. \tag{10.1}$$

The scaling (2.12) gives the parameter-free classical map M:

$$M: \begin{aligned} x_{n+1} &= x_n + y_n \\ y_{n+1} &= y_n - x_{n+1}^3 . \end{aligned} \tag{10.2}$$

Application of the same scaling to the quantum map (2.9) shows this to depend only on the single parameter $\hbar AT^3/\mu^2$, which will henceforth be denoted simply by $\hbar$.

The unperturbed region of M is the neighborhood of the origin. There, points move round contours of the scaled time-averaged Hamiltonian

$$\tfrac{1}{2}x^2 + \tfrac{1}{4}y^4 = \mathscr{E}. \tag{10.3}$$

It is these quartic curves $\mathscr{C}_0$ that will be iterated by M. The scaled energy is not the most convenient parameter, and we employ the action $I(\mathscr{E})$ for later quantization via (7.1). I is given by

$$\begin{aligned} I(\mathscr{E}) &= \frac{1}{2\pi}\oint p\, dq = \frac{2}{\pi}\int_0^{(4\mathscr{E})^{1/4}} \left(2\mathscr{E} - \frac{x^4}{2}\right)^{1/2} dx \\ &= \frac{2^{1/2}}{3\pi^{3/2}}\,\Gamma^2\left(\frac{1}{4}\right)\mathscr{E}^{3/4} = 1.11284\mathscr{E}^{3/4}. \end{aligned} \tag{10.4}$$

Another parameter useful in computation is the intercept $x_0 = (4\mathscr{E})^{1/4}$ of the $\mathscr{E}$ contours with the x axis; in terms of x_0,

$$I = 0.39345x_0^3. \tag{10.5}$$

The rotation number r of motion round the unperturbed curves (10.3) is $\omega T/2\pi$, which, since the scaling corresponds to $T = 1$ and $\omega = \partial\mathscr{E}/\partial I$, is

$$\begin{aligned} r &= \frac{1}{2\pi}\frac{\partial\mathscr{E}}{\partial I} = 0.19069\mathscr{E}^{1/4} \\ &= 0.18401I^{1/3} = 0.13484x_0 . \end{aligned} \tag{10.6}$$

For iteration under the quantum map we choose initial waves $\psi_0^{(k)}(x)$ that are the kth eigenstates of the quantum Hamiltonian corresponding to (10.3). To ensure semi-classical correspondence of $\psi_0^{(k)}$ with a given quartic curve $\mathscr{C}_0$ labelled by I, we choose

$$\hbar = I/(k + \tfrac{1}{2}). \tag{10.7}$$

Then $\psi_0^{(k)}(x)$ is computed by numerical integration of Schrödinger's equation.

First, we study the classical map M. Figure 9a shows a synoptic view of the phase plane x, y, obtained by iterating points with initial positions x_0, 0 for various x_0. Close to the origin, points lie on smooth invariant curves, whose existence follows from the Kolmogorov–Arnol'd–Moser theorem [1–4] and the fact that the pertur-

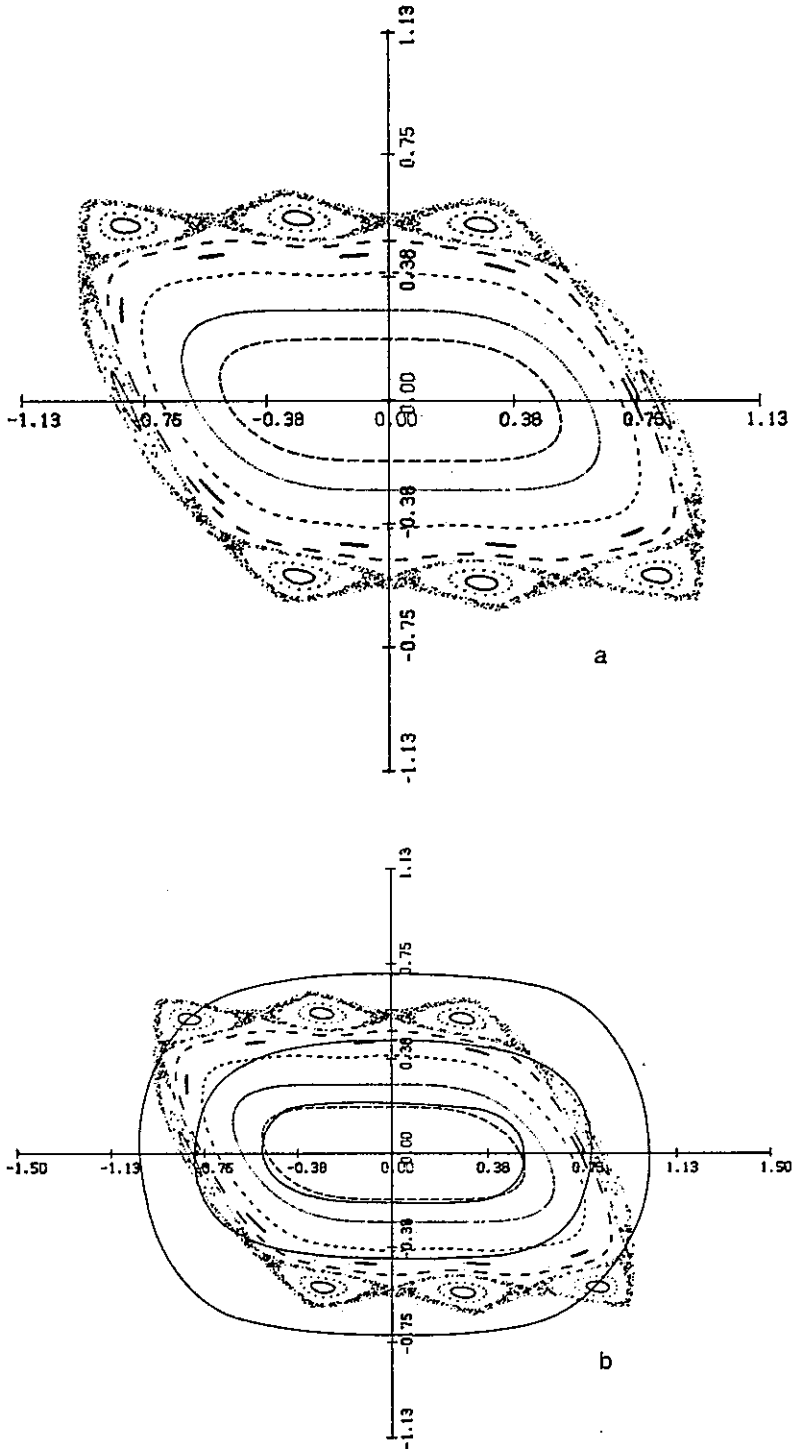

FIG. 9. (a) Synoptic view of the phase plane xy for the quartic map, made by iterating points $(x_0, 0)$ for several values of x_0; (b) The same as (a), but with three contours $\mathscr{C}_0$ of the unperturbed quartic Hamiltonian, for $x_0 = 0.53$, 0.78, and 1.00, superimposed on the point maps.

bation is small there (i.e., M is close to the integrable map generated by (10.3)). Even this apparently smooth region is broken up by elliptic islands and stochastic regions near places where r is rational for the unperturbed map. However, these regions must be of very small measure because r is small and, hence, can pass through only very high-order rationals; they are not resolved on Fig. 9.

When $x_0 = 0.74$ the first chain of islands can be discerned; there are nine of them, so that they originate in the unperturbed curve with $r = \frac{1}{9}$. (The rotation number of the unperturbed curve actually passing through $x_0 = 0.74$ is $r = 1/10.02$; the perturbation has shifted the curve $r = \frac{1}{9}$ as well as breaking it up.) For $0.78 < x_0 < 0.84$ points map round a chain of eight islands centered on elliptic fixed points and a stochastic region containing eight hyperbolic fixed points. When $x_0 > 0.84$ the perturbation is so large that all points escape to infinity rather than form the chains of islands that would correspond to larger r (lower-order rationals) in the unperturbed map.

We know no map on the infinite xy plane which exhibits stochasticity and for which no points escape. In a search for one, we studied maps generated by potentials

$$V(x) = \frac{\beta}{2}\left(x^2 - \beta \ln\left(1 + \frac{x^2}{\beta}\right)\right) \quad \text{and} \quad V(x) = \frac{x^4}{4 + 2x^2/\beta}, \tag{10.8}$$

which for small x, y tend to (10.2) and which asymptotically approach elliptic linear maps with rotation numbers r_∞ given by

$$\beta = 4 \sin^2 \pi r_\infty . \tag{10.9}$$

These did exhibit stochasticity, but points for which x_0 or y_0 was sufficiently great always excaped, albeit slowly. A brief study of a map whose approach to asymptotic linearity was exponentially fast showed that points did not escape, but failed to discover any stochastic regions; it seemed that the map is integrable, behavior reminiscent of the three-particle Toda "lattice" [3, 4].

Now we present iterations by M of three quartic curves $\mathscr{C}_0$ with $x_0 = 0.53$, 0.78, and 1.00, shown in Fig. 9b superimposed on the point maps.

For $x_0 = 0.53$, (corresponding to $\mathscr{E} = 0.020$, $I = 0.059$), $\mathscr{C}_0$ lies wholly within the "integrable" region covered with smooth invariant curves of M. Since these surround the elliptic fixed point at the origin O, away from which r varies smoothly, the iterates $\mathscr{C}_n$ will generate a whorl as explained in Section 6. Figure 10a shows some early states of its (slow) development.

For $x_0 = 0.78$ (corresponding to $\mathscr{E} = 0.091$, $I = 0.18$), $\mathscr{C}_0$ passes through some of the outermost hyperbolic fixed points and close to elliptic islands, as well as cutting invariant curves surrounding O. Figure 11a shows some of the iterates $\mathscr{C}_n$. They are dominated by a whorl from the elliptic point at O, which develops faster than that on Fig.10a because of the larger rotation number differences. On $\mathscr{C}_{15}$ subwhorls round the elliptic islands are starting to appear, and have evolved a little more on $\mathscr{C}_{20}$. There can also be discerned on $\mathscr{C}_{20}$ some nascent tendrils near the hyperbolic

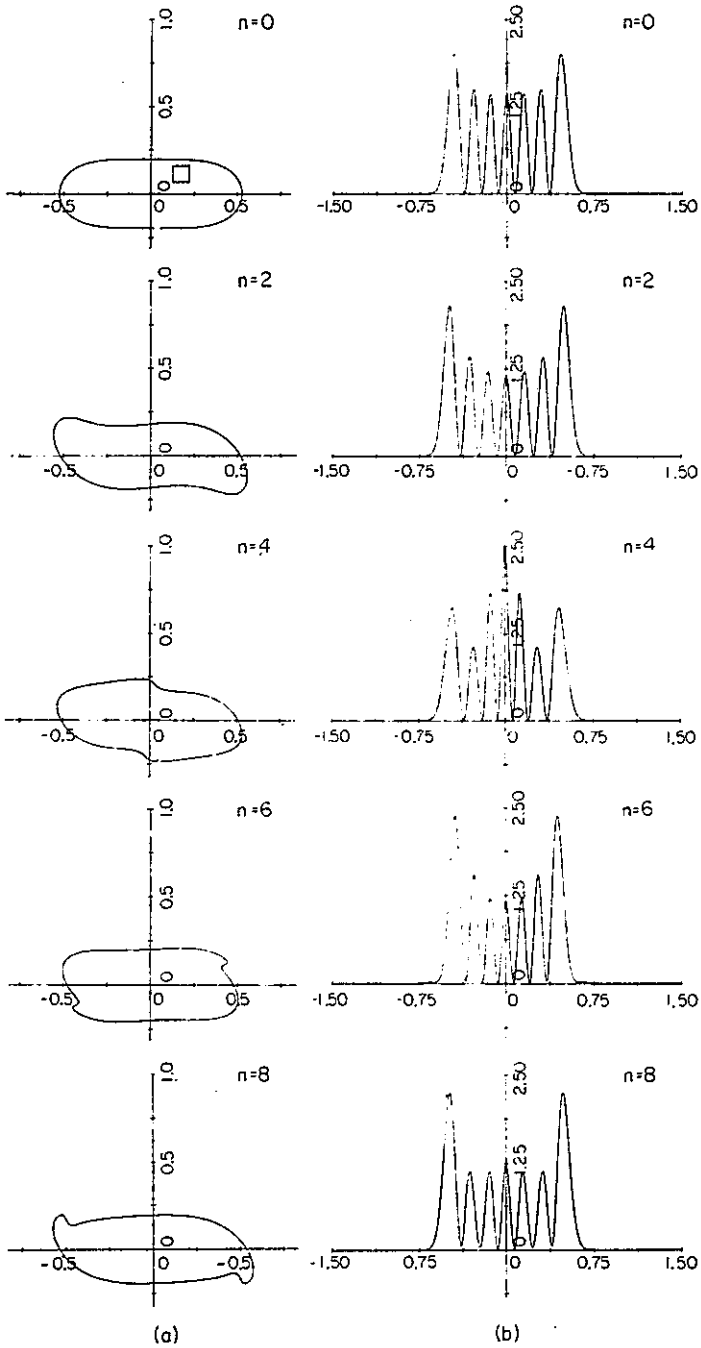

FIG. 10. (a) Classical maps $\mathscr{C}_n$ of initial curve $\mathscr{C}_0$ with $x = 0.53$ ($\mathscr{E} = 0.020$, $I = 0.059$) showing slowly developing whorl. (b) Quantum maps $|\psi_n^{(6)}(x)|^2$ of an initial wave $|\psi_0^{(6)}(x)|^2$ that is an eigenfunction of the unperturbed Hamiltonian $\bar{H}$. The area $\hbar$ (=0.0091) is marked as a square on (a).

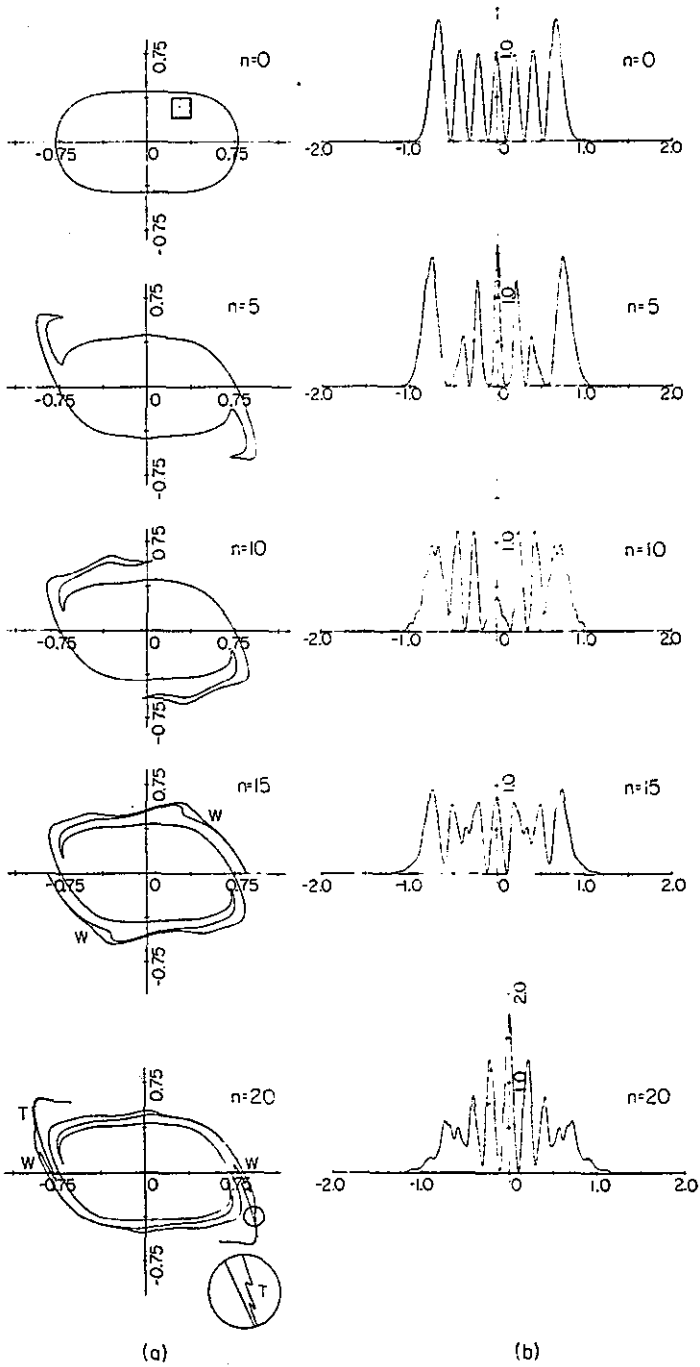

FIG. 11. (a) Classical maps $\mathscr{C}_n$ of initial curve $\mathscr{C}_0$ with $x = 0.78$ ($\mathscr{E} = 0.091$, $I = 0.18$) showing large whorl about the origin and the beginnings of subwhorls (W) for $n = 15$, 20 and tendrils (T) for $n = 20$. (b) Quantum maps $|\psi_n^{(6)}(x)|^2$ of an initial wave $|\psi_0^{(6)}(x)|^2$ that is an eigenfunction of the unperturbed Hamiltonian $\bar{H}$. The area $\hbar$ ($=0.028$) is marked as a square on (a).

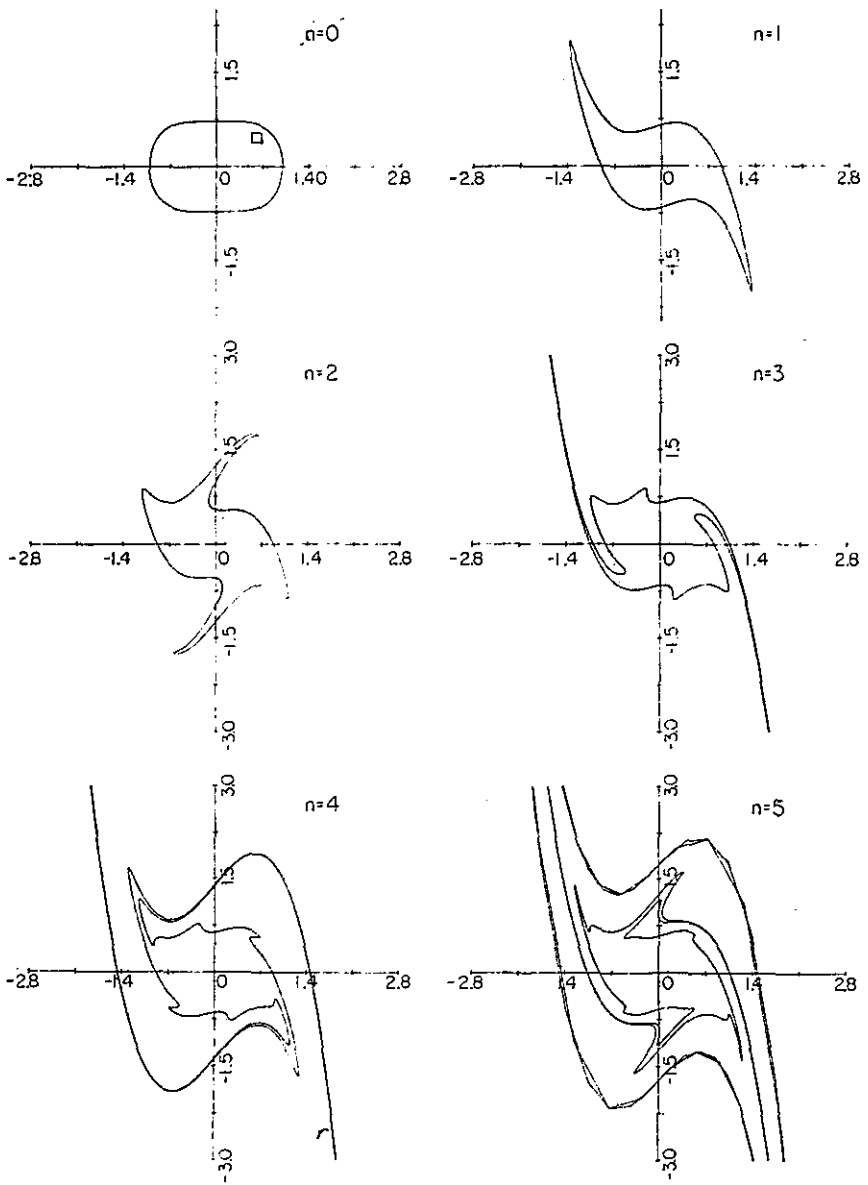

FIG. 12. (a) Classical maps $\mathscr{C}_n$ of initial curve $\mathscr{C}_0$ with $x = 1.00$ ($\varepsilon = 0.25$, $I = 0.40$) showing rapid growth of two tendrils. (b) Projection of (a) onto coordinate axis, showing proliferation of caustics. (c) Smoothing of (b) over distance 0.05. (d) Quantum maps $|\psi_n^{(18)}(x)|^2$ of an initial wave $|\psi_0^{(18)}(x)|^2$ that is an eigenfunction of the unperturbed Hamiltonian $\bar{H}$. The area $\hbar$ ($= 0.022$) is marked as a square on (a). (e) Smoothing of (d) over distance 0.05.

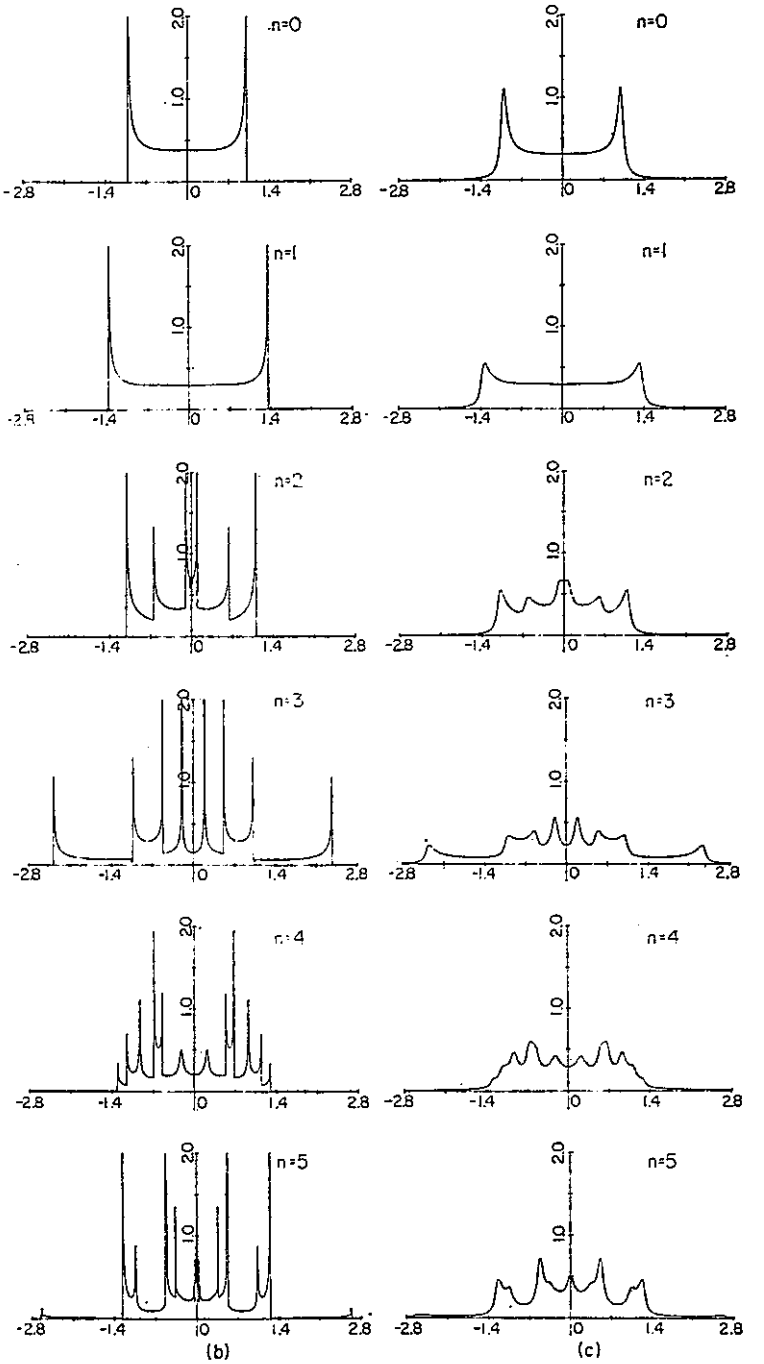

FIG. 12—*Continued*

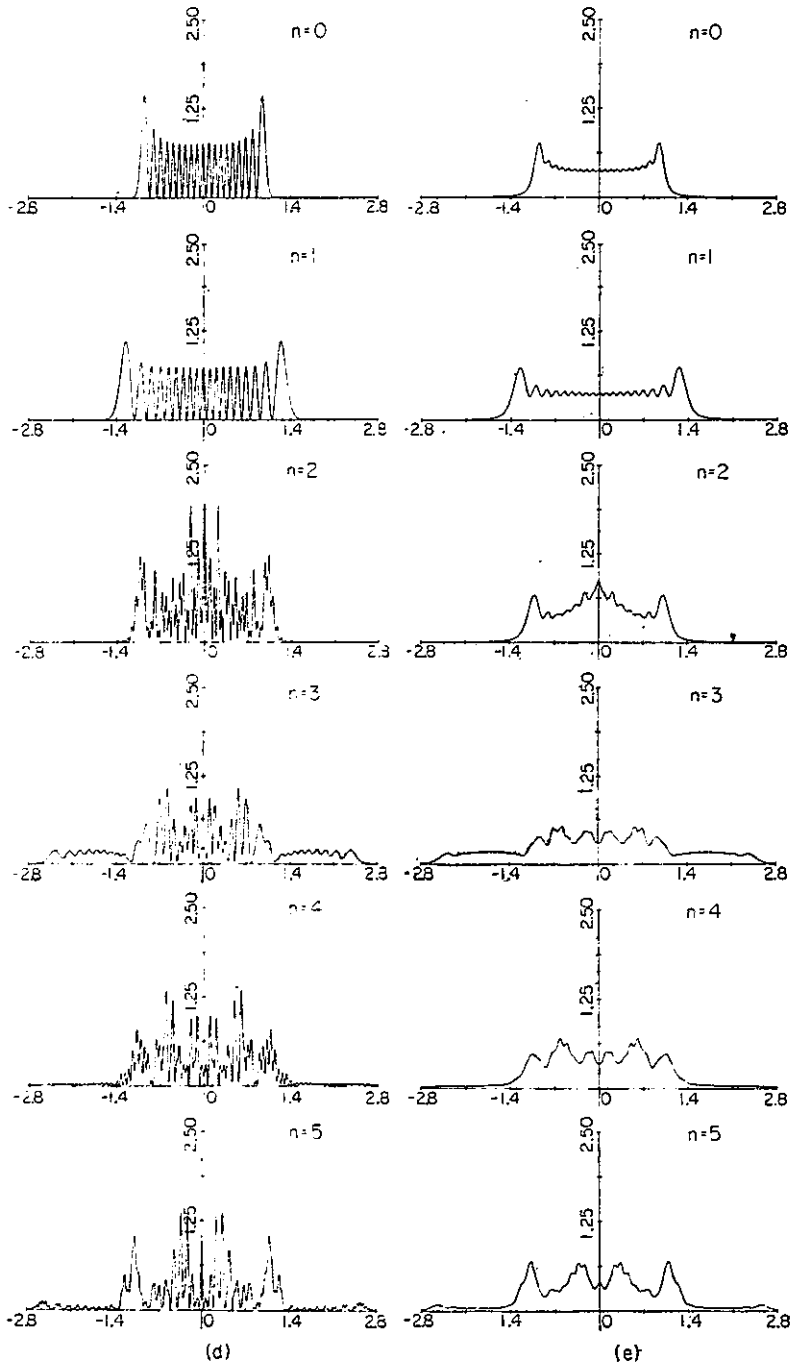

FIG. 12—*Continued*

points, as described in Section 6. They appear as regions of irregularity on the curve, with several undulations which, however, are on a very small scale because of the narrowness of the band of stochastic motion (Fig. 9a).

For $x_0 = 1.00$ ($\mathscr{E} = 0.25, I = 0.40$), $\mathscr{C}_0$ lies almost entirely in the unstable "escape" region, but does dip into the outer island chain, passing close to two elliptic and two hyperbolic points. The iterates $\mathscr{C}_n$, shown in Fig. 12a, are dominated by two rapidly growing tendrils swinging violently back and forth as they reach out to infinity. However, there is also rotation into a large whorl around O.

Now we study the quantum map, by numerical integration of wavefunctions under (2.9). First we iterate an eigenstate of the time-averaged Hamiltonian (10.3) corresponding to the curve $\mathscr{C}_0$ with $I = 0.059$, with quantum number $k = 6$. From (10.7), this implies $\hbar = 0.0091$. A square with area $\hbar$ has been marked on the first phase plane in Fig. 10a. The iterated probability densities $|\psi_n^{(6)}(x)|^2$ are shown in Fig. 10b. Because the convolutions of $\mathscr{C}_n$ (the beginnings of the whorl) do not have an area large in comparison with $\hbar$, they do not have a dramatic effect on the form of $|\psi_n|^2$ which does not changed drastically under the map.

However, it is possible to see the caustics, where $|\psi_n|^2$ rises to large values. These correspond to turning points, where $\mathscr{C}_n$ is perpendicular to the x axis. They are quite strong for iterations 6 and 8 where several caustics or near-caustics lie close together near the extreme x values of $\mathscr{C}_n$. In iteration 4 the effect of the near-caustic close to the origin is clearly visible as the large central maximum of $|\psi_n|^2$.

It is also worth noting that the wavelength λ of the oscillations in Fig. 10b is in good agreement with the de Broglie rule $\lambda = h/y$, where y is the corresponding momentum on $\mathscr{C}_n$. Near $x = 0$ this predicts $\lambda \approx 0.3$.

Further iteration of this quantum map up to $n = 20$ produced no new features because the corresponding curve map shows that the whorl is still at an early stage of its development.

Next we iterate a wave corresponding to the curve $\mathscr{C}_0$ with $I = 0.18$, again choosing $k = 6$. This implies $\hbar = 0.028$. A square with this area has been marked in Fig. 11a. The iterated quantum probability density is shown in Fig. 11b. Its form changes strikingly under the map, in marked contrast to Fig. 10b. Clearly this is a reflection of the fact that $\mathscr{C}_n$ is substantially convoluted on scales exceeding $\hbar$.

Now the caustics are not much in evidence, except for $|\psi_5|^2$ where they obviously arise from the thick arms of $\mathscr{C}_5$, which are almost perpendicular to the x axis. By iteration 20 the curve has such a confusion of branches near the extreme x values that $|\psi_{20}|^2$ drops smoothly down to what may be the "anticaustics" recently predicted [13].

The mean oscillation wavelength λ (~ 0.4 near $x = 0$) is again given by de Broglie's rule, but now the convolutions of $\mathscr{C}_n$, giving multiple values of y for each x, cause ψ_n to lose its spectral purity. Evidence of the interference of different scales of oscillation can be seen on $|\psi_{10}|^2$, $|\psi_{15}|^2$, and $|\psi_{20}|^2$.

For a more thoroughgoing comparison between classical and quantum maps, we iterate a state with $k = 18$ corresponding to the escaping curve with $I = 0.40$. Now $\hbar = 0.022$. Again a square with this area has been marked in Fig. 12a. The iterations

$|\psi_n^{(18)}(x)|^2$ are shown in Fig 12d. Now the evolution away from ψ_0 is dramatic and reflects the evolution of $\mathscr{C}_n$ (Fig. 12a) in several ways:

Perhaps the most striking feature is the multiple scales of oscillation of ψ, beginning at iteration 2 when $\mathscr{C}_n$ first develops extra turning points. Then there is the leakage of the wave to large $|x|$, beginning at iteration 3 when $\mathscr{C}_n$ first sends out long tendrils; computationally, this is also evident in a gradual diminution of the normalization integral over the finite x range considered, as n increases.

For a systematic study of the caustics we project $\mathscr{C}_n$ onto the x axis as explained in Section 5 (cf. Eq. (5.21)), thus obtaining $|\psi_n|^2_{\text{classical}}$. This projection must be carried out using the correct density on $\mathscr{C}_n$, which is that arising under M from a density on $\mathscr{C}_0$ that is uniform in the "angle" variable θ. θ is proportional to the travel time of points round $\mathscr{C}_0$ and is defined by

$$\theta = \omega(I)t = 2^{-1/2}\frac{\partial \mathscr{E}(I)}{\partial I}\int_{(4\mathscr{E})^{1/4}}^{x_0}\frac{dx}{(\mathscr{E} - \frac{1}{4}x^4)^{1/2}}. \tag{10.10}$$

This gives $x_0(\theta)$ and $y_0(\theta)$ $(=[2\mathscr{E} - \frac{1}{2}x_0^4]^{1/2})$ parametrically in terms of θ for the curve $\mathscr{C}_0$ labeled by $\mathscr{E}$. Then the correct procedure is to iterate x_0 and y_0 under M to get $x_n(\theta)$, $y_n(\theta)$, and the projection of $\mathscr{C}_n$ is (cf. (7.4))

$$|\psi_n(x)|^2_{\text{classical}} = \frac{1}{2\pi}\sum_i \left|\frac{dx_n(\theta_i(x))}{d\theta}\right|^{-1}. \tag{10.11}$$

where $\theta_i(x)$ are those angles θ giving the different branches of $\mathscr{C}_n$ at x.

These projections are shown in Fig. 12b. Caustic spikes dominate, and proliferate rapidly on iteration (there are more than 20 when $n = 5$). The general apparance of the projections is not very similar to the exact quantum probability densities of Fig. 12d. In particular for $n \geqslant 2$ there is no clear relationship between individual caustics and features of $|\psi_n|^2$. The reason is that the caustics are clustered closer than the mean de Broglie wavelength λ ($\sim$0.2).

In these circumstances we employ the smoothing device described in Section 5, averaging both the exact $|\psi_n|^2$ (Fig. 12e) and $|\psi_n|^2_{\text{classical}}$ (Fig. 12c) over a distance comparable with λ. So as not to average away too much interesting structure we use the conservative smoothing distance 0.05 ($\sim\frac{1}{4}\lambda$). This final comparison between quantum and classical mechanics is most encouraging. Good agreement between Figs. 12c and e persists through the "stochastic transition" ($n \sim 2$ or 3) separating two morphologically distinct sorts of wavefunction. Before the transition, ψ_n is dominated by a few interfering waves of the form (5.2), with occasional caustics. After the transition, ψ_n is dominated almost everywhere by clusters of caustics. Since caustics are catastrophes [37, 34], we can say, epigrammatically:

"Stochasticity is the ubiquity of catastrophe".

The interpretations and conclusions in this section are reinforced by a great many more computations, which shortage of space prevents our showing here. In addition

to $|\psi_n|^2$, we have plotted Re ψ_n, Im ψ_n, and the momentum wavefunction (which is the Fourier transform of ψ_n).

11. Conclusions

In this paper we have quantized a class of generic area-preserving maps of the phase plane. The resulting quantum maps provide a promising way of studying, in systems with one degree of freedom, semiclassical effects which on more conventional models only appear when the number of degrees of freedom is at least two. The advantage of this is that classical motion can be depicted in the qp plane, and quantum wavefunctions plotted in the ψ, q plane, instead of having to be studied in sections as for more degrees of freedom. Therefore, the development of classical and quantum stochasticity can be followed in detail.

The classical feature most affecting the develoopment of quantum states ψ_n is the increasing complication of classical curves $\mathscr{C}_n$, whose principal morphology (Section 6) is convolutions of two types that we call whorls and tendrils. We hope this work will encourage people to study in more details mappings of curves rather than points.

When the convolutions of $\mathscr{C}_n$ become so fine as to have areas h or smaller, ψ_n undergoes a transition to a different morphology, as indicated by the theoretical arguments of Section 5 and illustrated in computations of Section 10. This morphology has not previously been studied in semiclassical analysis, and there is much scope for further research to elucidate its details. On the simplest level, our demonstration of the close agreement between the smoothed classical probability density (Fig. 12c) and smoothed exact quantum probability density (Fig. 12e) shows $|\psi_n|^2$ to be dominated by dense clusters of caustics. On finer scales, arguments given elsewhere [13] show how the pattern of local oscillations of $\psi_n(x)$ (in particular its spectrum and autocorrelation function) can be obtained from $\mathscr{C}_n$ even when this is complicated. Perhaps $\mathscr{C}_n$, with complication on all scales through h, can be considered as a fractal curve [38], and ψ_n as a "diffractal" [39].

There is a need for exact theorems about the eigenstates of quantum maps. Clearly Eq. (2.9) admits a greater richness of behavior than the familiar time-independent Schrödinger second-order differential equation. We do not even know under what circumstances the spectrum of eigenvalues α is discrete. Presumably this is connected with the boundedness of orbits in the classical map M. Perhaps the fact that in the quartic and other maps we have studied there is a central bounded region, outside of which points escape to infinity under iteration, means that the quantum spectrum has narrow resonances rather then true discrete states. If discrete states ϕ_k do exist, is there a simple relation between the ordering of α_k and the nodal structure of $\phi_k(q)$, as in the harmonic case that we solved exactly (Section 8)? One way to ensure boundedness is to close the phase plane into the torus T. The simplest map on T is Arnold's cat [1, 3, 4], which is totally stochastic. We have succeeded in quantizing this and will publish the results elsewhere [31].

ACKNOWLEDGMENTS

We thank Dr. J. H. Hannay for helpful discussions, Professor G. Casati and Professor J. Ford for informing us of related work [19] prior to publication, and Professor R. Marcus for his generous provision of computer facilities.

REFERENCES

1. V. I. ARNOL'D, *Usp. Mat. Nauk.* **18** (1963), No. 5, 13–39, No. 6, 91–196 (English translations in *Russ. Math. Surv.* **18** (1963), No. 5, 9–36, No. 6, 85–191); V. I. ARNOL'D AND A. AVEZ, "Ergodic Problems of Classical Mechanics," Benjamin, New York, 1968.
2. J. MOSER, *Mem. Amer. Math. Soc.* **81** (1968).
3. J. FORD, *in* "Fundamental Problems in Statistical Mechanics III" (E. G. Cohen, Ed.), pp. 215–255, North–Holland, Amsterdam, 1975.
4. M. V. BERRY, *in* "Topics in Nonlinear Dynamics" (S. Jorna, Ed.), *Amer. Inst. Phys. Conf. Proc. Series*, Vol. 46, Chap. 2, AIP, New York, 1978.
5. A. EINSTEIN, *Verh. Dev't. Phys. Ges.* **19** (1917), 82–92.
6. J. B. KELLER, *Ann. Phys.* 4 (1958), 180–188.
7. V. P. MASLOV, "Theorie des Perturbations et des Methodes Asymptotiques," Dunod, Paris, 1972 (original Russian edition, 1965).
8. A. VOROS, *Ann. Inst. H. Poincare, A* **24** (1976), 31–90.
9. I. C. PERCIVAL, *Advan. Chem. Phys.* **36** (1977), 1–61.
10. M. C. GUTZWILLER, *J. Math. Phys.* **12** (1971), 343–358; *in* "Path Integrals and Their Applications," Proceedings, NATO Conference, Antwerp, 1977, in press.
11. I. C. PERCIVAL, *J. Phys. B* 6 (1973), L229–232.
12. A. VOROS, *Ann. Inst. H. Poincare A* **26** (1977), 343; *in* "Stochastic Behaviour in Classical and Quantum Hamiltonian Systems" (G. Casati and J. Ford, Eds.), Lecture Notes in Physics, Springer-Verlag, New York/Berlin, in press.
13. M. V. BERRY, *J. Phys. A* **10** (1977), 2083–2091.
14. K. S. J. NORDHOLM AND S. A. RICE, *J. Chem. Phys.* **61** (1974), 203–223, 768–779.
15. (a) I. C. PERCIVAL AND N. POMPHREY, *Mol. Phys.* **31** (1976), 97–114; (b) N. POMPHREY, *J. Phys. B* 7 (1974), 1909–1915.
16. N. C. HANDY, S. M. COLWELL, AND W. H. MILLER, *Faraday Disc.*, No. 62 (1977), 29.
17. D. W. NOID AND R. A. MARCUS, *J. Chem. Phys.* **62** (1975), 2119–2124.
18. J. MOSER, *Nach. Akad. Wiss. Goettingen* **1** (1962), 1–20; "Stable and Random Motions in Dynamical Systems," Princeton Univ. Press, N.J., 1973.
19. G. CASATI, B. V. CHIRIKOV, F. M. IZRAELEV, AND J. FORD, *in* "Stochastic Behabiour in Classical and quantum Hamiltonian Systems" (G. Casati and J. Ford, Eds.), Lecture Notes in physics, Springer–Verlag, New York/Berlin, in press.
20. D. MARCUSE, "Light Transmission Optics," Van Nostrand, Princeton, N.J., 1972.
21. J. MOSER, *Bol. Soc. Mat. Mex.* (1960), 176–180.
22. E. P. WIGNER, *Phys. Rev.* **40** (1932), 749–759; H. J. GROENEWOLD, *Physica* **12** (1946), 405–460; J. E. MOYAL, *Proc. Cambridge Phil. Soc.* **45** (1949), 99–124; T. TAKABAYASI, *Progr. Theor. Phys. Japan.* **11** (1954), 341–373; G. A. BAKER, JR., *Phys. Rev.* **109** (1958), 2198–2206.
23. E. J. HELLER, *J. Chem. Phys.* **67** (1977), 3339–3351.
24. M. V. BERRY, *Phil. Trans. Roy. Soc. London Ser. A* **287** (1977), 237–271.
25. M. V. BERRY AND N. L. BALAZS, *J. Phys. A* **12** (1979), 625–642.
26. N. L. BALAZS AND G. G. ZIPFEL, JR., *Ann. Phys. (New York)* **77** (1973), 139–156.
27. M. ABRAMOWITZ AND I. A. STEGUN, "Handbook of Mathematical D.C., Functions," U.S. National Bureau of Standards, Washington, 1964.
28. C. CHESTER, B. FRIEDMAN, AND F. URSELL, *Proc. Cambridge Phil. Soc.* **53** (1957), 599–611.

29. V. I. ARNOL'D, *Funkt. Anal. Ego. Pril.* 6 (1972), 12–20 (English translation in *Funct. Anal. Appl.* 6 (1972), 94–101).
30. M. V. BERRY AND M. TABOR, *Proc. Roy. Soc. London Ser. A* 349 (1976), 101–123; and *J. Phys. A* 10 (1977), 371–379.
31. M. V. BERRY AND J. H. HANNAY, to be published.
32. P. A. M. DIRAC, "The Principles of Quantum Mechanics," Oxford Univ. Press (Clarendon, London/New York, 1947.
33. D. LUDWIG, *Commun. Pure Appl. Math.* 19 (1966), 215–250.
34. M. V. BERRY, *Advan. Phys.* 25 (1976), 1–26.
35. M. V. BERRY AND K. E. MOUNT, *Rep. Progr. Phys.* 35 (1972), 315–90.
36. YY B. ZEL'DOVICH, *Sov. Phys. JETP* 24 (1967), 1006–1008.
37. T. POSTON AND I. STEWART, "Catastrophe Theory and Its Applications," Pitman, London, 1978.
38. B. B. MANDELBROT, "Fractals," San Francisco, Freeman, 1977.
39. M. V. BERRY, *J. Phys. A* 12 (1979), 781–797.
40. G. M. ZASLAVSKII AND N. N. FILONENKO, *Sov. Phys. JETP* 38 (1974), 317–323.
41. G. P. BERMAN AND G. M. ZASLAVSKII, *Physica A* 91 (1978), 450–460.
42. T. B. SMITH, *J. Phys. A* 11 (1978), 2179–2190.
43. A. J. LICHTENBERG, "Phase Space Dynamics of Particles," p. 95, Wiley, New York, 1969.

Printed by the St. Catherine Press Ltd., Tempelhof 37, Bruges, Belgium